November 2022

Stochastic Models for Resilience Assessment and Improvement

Weimar Ardila Rueda
University of South Florida

Stochastic Models for Resilience Assessment and Improvement

by

Weimar Ardila-Rueda

A dissertation submitted in partial fulfillment
of the requirements for the degree of
Doctor of Philosophy
Department of Industrial and Management Systems Engineering
College of Engineering
University of South Florida

Major Professor: Alex Savachkin, Ph.D.
Walter Silva-Sotillo, Ph.D.
Kingsley Reeves, Ph.D.
Alex Volinsky, Ph.D.
Daniel Romero-Rodriguez, Ph.D.

Date of Approval:
November 18, 2022

Keywords: Resilience Enhancement, Post-disruption Response, Resource Allocation,
Markov Decision Process, Dynamic Programming

Dedication

As with any other life-changing event, the Ph.D. is a continuous learning process with ups and downs, where new challenges always come up at a constant rate, as in a Poisson process. This dissertation is dedicated to all the people who have encouraged me to be more resilient during this long journey: my beloved wife, my incredibly hardworking parents, my family and friends from my native Colombia, and my professors. I greatly appreciate all their support and guidance.

Acknowledgments

First and foremost, I would like to acknowledge my major professor Dr. Alex Savachkin for his constant guidance and support throughout all these years. It has been nothing less than a pleasure to work under his wise supervision. Dr. Savachkin is highly likely the most meticulous person I have ever met, encouraging me to develop and work on my research ideas methodically, and from whom I have learned and still learning the most.

I would also like to extend my gratitude to Dr. Daniel Romero-Rodriguez, a source of unconditional support and a role model of passion and professionalism. I am also enormously grateful to the IMSE department at USF for allowing me to be part of an amazing and enthusiastic group of Ph.D. students.

I wish to thank my family, especially my parents, Moises and Yolanda, for their tireless efforts and sacrifices to grant me the best possible education they could. Finally, to my wife, Roxana, whose company has been for me the driver to overcome adversities and become a more resilient person.

Table of Contents

List of Tables

List of Figures

Abstract

Resilience refers to the ability of a system to absorb and mitigate the impact of potential disruptions and return to normal operational conditions. The above notion of resilience allows us to distinguish two stages in a system's post-disruption response, the absorptive dimension and the recovery dimension [6]. The absorptive dimension is related to a system's robustness and capacity to mitigate initial loss posterior to a disruption. Meanwhile, the recovery dimension is the system's rapidity to return and reach an acceptable level of functionality after the disruption occurrence [7].

A social-physical (SP) system's post-disruption response is related to its resilience capacity so building more resilient systems is the key to managing and dealing with unexpected disruptions. However, many resilience actions typically involve economic impacts, which limit their implementation [6]. This problem has been documented in different contexts. For example, during the early stages of pandemic mitigation, strict lockdowns are effective against virus propagation but may lead to harmful economic effects in the communities [8]. Therefore, finding a balance between being resilient and the costs of being resilient is essential.

This dissertation proposes implementing stochastic dynamic optimization models based on an infinite horizon Continuous-Time Markov Decision Processes to balance the intervention investment and enhance an SP system's overall resilience. We do so by reducing the initial drop in performance and the recovery time during the post-disruption response. Since the system's evolution is progressive and involves uncertainty, we can model the system response as a Markov process.

In the models' formulation, we use common elements in resilience literature to provide a broader framework that facilitates the application in different disruption scenarios. For

our state-space definition, we use the idea that in high-magnitude events with long recovery times, the recovery process can be modeled by considering multiple performance intervals. On the other hand, actions and rewards are related to the investment required to guarantee a transition between states. We assess the model's performance using testbeds based on different disruption scenarios, such as natural disasters and pandemic outbreaks. The proposed model can provide policymakers with information on the optimal recovery strategy and how to allocate resilience resources during the post-disruption response.

Chapter 1: Introduction

Resilience refers to the ability of a system to absorb and mitigate the impact of potential disruptions and return to normal operational conditions. This ability is critical for disaster management in social-physical systems such as large or small communities, supply networks, or companies in the middle of highly competitive environments [9].

During the past years, highly intense disruptions like the 2022 and 2017 Hurricanes Ian and Irma [10, 11], the COVID-19 pandemic outbreak [8, 12], the 2011 Great East Japan Earthquake [13], and the 2010 Dique Canal breach in Northern Colombia [1] have revealed the vulnerability of social-physical systems and their struggles during the mitigation process. Moreover, the damage to critical infrastructure due to a natural disaster (e.g., water and wastewater, electric power, transportation, etc.) or the strict lockdown measures and saturation of healthcare systems during a pandemic may lead to significant societal and economic impacts [14, 8]. Those negative impacts highlight the relevance of building more resilient systems to ensure their regular performance and withstand future disruptions.

Nonetheless, from an economic perspective, many resilience strategies conflict with traditional business goals [6], making their implementation a complicated task (or even meaningless) if there is no proper balance between being resilient and the costs of being resilient. We can extend this statement to other contexts as well. For instance, effective and rapid relief logistics are essential to lessen casualties and property losses in post-disaster emergency response. However, natural disasters usually disrupt power supplies, communications, and transportation infrastructure, making the system's response progressive and slow. This situation demands strategic decisions to deliver relief supplies to impacted areas and deal with the lack of critical resources [15]. On the other hand, in a pandemic outbreak, aggressive

lockdown measures to reduce virus propagation and mitigate the saturation of healthcare services may produce significant economic impacts on communities, such as an increment in the unemployment rate, small business bankruptcy, and supply problems [8, 12]. Under this scenario, myopic approaches to decision-making that only focus on lessening the infected number may be as damaging as the pandemic itself.

Resilience enhancement models (e.g., resource allocation models) drive decision-makers towards the resilience dimension where the intervention is necessary to boost the performance and reduce disruptions impacts [16]. In addition, these models enable investment prioritization when multiple hardening and recovery actions are available. For instance, many resource allocation models have been developed in disaster management to strengthen and restore a system while facing natural disasters or man-made disruptions. Thence, optimal resource allocation to increase resilience levels is essential for supporting decision-makers in the strategy selection [3].

This research aims to provide a Continuous-Time Markov Decision Process (CTMDP) model to enhance a physical system's global resilience by accelerating its recovery process. We apply and evaluate the model using two testbeds under different disruption scenarios, the 2010 Dique Canal breach in Colombia [1], and a pandemic influenza outbreak [17, 5, 18]. The model considers parameters that, in a real-world context, are easy to monitor and track during a system's evolution within the post-disruption process, such as the performance level and recovery time [19]. The main objective is to minimize the cost of implementing actions that reduce the initial performance loss and recovery time. Furthermore, the formulation considers multiple performance levels to capture the system evolution during the mitigation and recovery stages [1].

Our research contributions center on the following aspects:

- Introducing a broader framework for resilience enhancement to facilitate decision-making in different disruption scenarios and systems types. We do so by focusing on either the absorptive (performance loss) or recovery (restoration time) dimension

of the post-disruption response and considering the hidden costs of having a disrupted system.

- Balancing the costs of resilience improvement by considering both the costs of intervention and the costs of having a disrupted system. This aspect is essential to ensure a realistic implementation of resilience actions and reduce the economic impacts of that implementation.

- Establishing decision guidelines for balancing the costs of the resilience by providing a stochastic optimization model for the dynamic allocation of resilience resources during the mitigation process to deliver a more proactive control in the post-disruption response.

This dissertation has been organized as follows: Chapter 2 presents the literature review section that focuses on the foremost common approaches in mostly resilience models, dynamic control models, and relevant resilience assessment tools. Chapter 3 describes the overall and specific research objectives. Then, in Chapter 4, we provide the details of our Markov decision process (MDP) model, including the definition of the state/action space, state transition matrix, cost function, and optimality framework. Afterward, Chapter 5 discusses a CTMDP-based implementation of our Dique Canal testbed and provides further insights into the testbed analysis by examining optimal recovery policies using a Markov Chain Monte Carlo (MCMC) simulation. Chapter 6 discusses a CTMDP-based implementation of our pandemic mitigation testbed, where slight modifications in the original formulation are considered to capture the dynamics of a pandemic testbed. We also assess the performance of the optimal mitigation policy via MCMC. Finally, Chapter 7 discusses the conclusions and future directions.

Chapter 2: Literature Review

Most resilience models are based on deterministic optimization techniques or focus on the resilient assessment rather than practical issues such as intervention cost balance and resource management [6]. Notwithstanding that the motivation behind measuring resilience typically focuses on helping decision-makers to define the best possible reaction when facing a disruption, there is a lack of attention to the balance between preparing a resilient system and the resources needed to achieve it [16]. Table 2.1 shows this gap in the literature. So, one of our concerns in this work is how to allocate resources to improve the post-disruption response and enhance a system's resilience (see Figure 2.1).

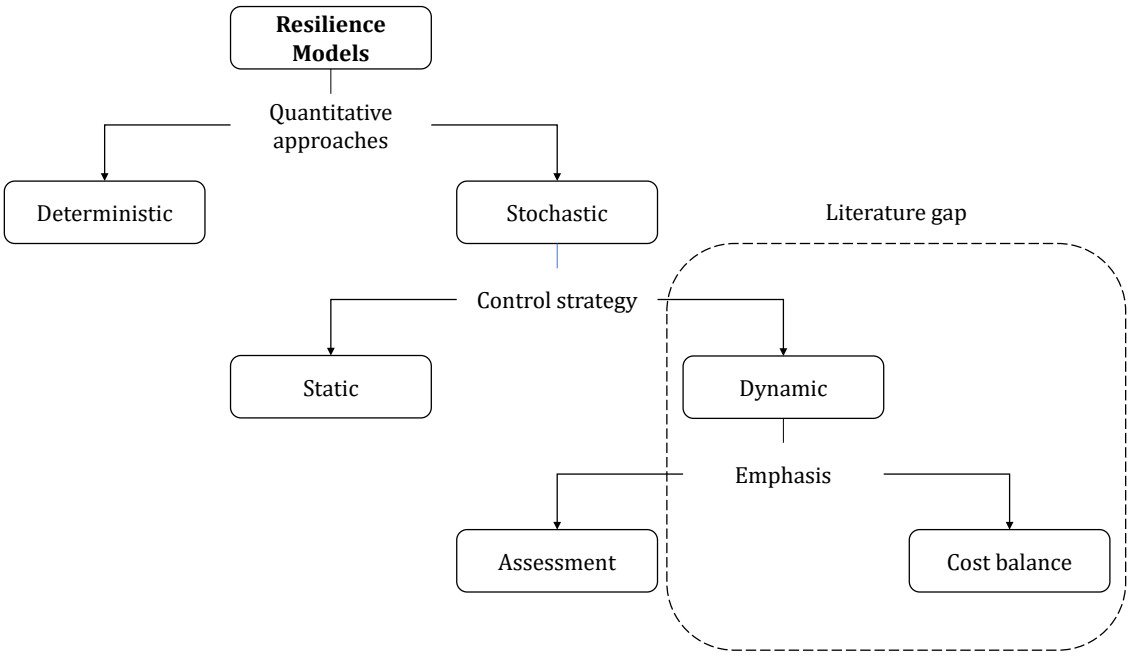

Figure 2.1: Resilience models: general classification

Table 2.1: Resilience models: literature summary

Authors	Year	Model		Control		Emphasis		Testbed Type
		Deterministic	Stochastic	Static	Dynamic	Resilience Assessment	Costs Balance	
Bruneau [7]	2003	✓		✓		✓		PS
Chuat et al [20]	2005							-
Cimellaro et al [21]	2010	✓		✓		✓		PS
Zobel et al [22]	2010	✓		✓		✓		PS
Zobel et al [23]	2014	✓		✓		✓		PS
Ouyang [24]	2012		✓	✓		✓		PS
Ouyang [25]	2015		✓	✓		✓		PS
Boochini & Frangopol [26]	2012	✓		✓		✓	✓	P
Rouge et al [27]	2013		✓		✓	✓		E
Pant et al [28]	2014		✓	✓		✓		P
Ayyub [29]	2015		✓	✓		✓		-
Zhang et al [30]	2015		✓	✓		✓		PS
Alderson et al [31]	2015	✓		✓				P
MacKenzie et al [16]	2016		✓	✓			✓	PS
Njilla et al [32]	2018		✓		✓			-
Clark et al [33]	2017		✓		✓			CP
Romero & Savachkin [3]	2018	✓		✓		✓		PS
Romero et al [1]	2019	✓		✓			✓	PS
Hulse et al [34]	2018	✓				✓	✓	P
Guidotti et al [14]	2020		✓			✓		PS
Kammouh et al [35]	2020		✓			✓		PS
Liu et al [36]	2021		✓					P
Sun et al [15]	2021		✓					PS
Geng et al [37]	2022		✓			✓	✓	PS
Iannacone et al [38]	2022		✓			✓		PS

"P": Physical "S": Social "C": Cyber "E": Ecological "-": No specified

The literature review begins with a discussion of quantitative models' approaches for impact mitigation and resilience assessment. These approaches are classified into deterministic and stochastic models [39], depending on their assumptions regarding the uncertainty in parameters like the initial performance loss, failure time, or disruption intensity. Afterward, we present a brief review of mitigation/control strategies emphasizing dynamic control models for enhancing resilience. Finally, we focus our discussion on the resilience assessment and the implementation of resilience metrics for system monitoring and decision support.

2.1 Resilience Models' Approach

Usually, resilience models scope their analysis in critical parameters such as the initial performance loss, recovery time, intervention cost, and disruption intensity [3]. Depending on the amount of information regarding those parameters, some may or may not assume random conditions. We classified the models approach into deterministic or stochastic based on those conditions [39].

Deterministic resilience models assume complete knowledge about disruption conditions and the system's reaction. Consequently, most concentrate on providing a predicted resilience assessment and resource allocation under specific scenarios. On the other hand, stochastic resilience models consider a more realistic behavior for failure modeling with probabilistic disruption scenarios and the randomness inherent to the recovery process.

Some of the deterministic models applications include the definition of a framework for the analytical quantification of disaster resilience [7, 21, 22], the characterization of multi-event disaster resilience [40, 23], finding the best intervention schedule in bridges restoration through resilience costs optimization [26], the evaluation of the potential losses through quantitative modeling of a system operation [31], allocation to facilitate the post-disaster recovery [41], and resilience assessment based on a multi-stage recovery scenario [1].

The implementation of stochastic modeling is also a comprehensive approach in several ways. Some involve the quantification of resilience through time-based stochastic metrics

[28, 24, 25]. Others propose a set of practical resilience metrics based on a Poisson process framework [29] and the application of Bayesian networks [42]. Regarding resource allocation and cost reduction, [16] presents a model to enhance resilience before disruption where the initial loss and recovery time are unknown parameters. This last work also provides a resilience assessment metric as a function of the average loss per unit time needed to recover.

2.2 Dynamic Control Models

Most of the above models consider static control strategies, where decisions are fixed and do not vary according to the current system conditions. On the other hand, Markov decision processes (MDPs) provide a dynamic control framework for the decision-maker, where a resource allocation action may change depending on the current state and evolution of the system within the recovery process. This approach allows more proactive decision-making to improve the system's post-disaster response and increase the overall resilience. For instance, [27] based on the ecological definition of resilience and the viability theory for lakes eutrophication, built a discrete-time Markov model for resilience to minimize the recovery time. Likewise, [43] proposes an MDP formulation for computing recovery actions in a critical infrastructure system during seismic disruptions in a water network case study. In addition, some applications for Cyber-Physical Systems (CPS), such as the resilient design of autonomous systems [44], and the mathematical definition for intrusion resilience in CPS through the formulation of a hierarchical game between the targeted cyber-physical platform and a cyber adversary [33].

Nevertheless, there are relative few MDPs research works on applications for the dynamic allocation of resilience resources, and because of the lack of a consensus on the resilience definition and metrics [45, 19], each of them provides its framework for resilience definition and assessment. For instance, consider the set of ideal states and the resilience basin proposed by [27], and the security state space defined in the set of values $\{0, 1\}$ by [33]. In both cases, there is a state-space definition tailored to their notion of resilience and the unique features

of their testbeds that do not provide a general framework that can be easily expanded to other kinds of systems.

2.3 Resilience Assessment

In general, resilience metrics are based on the records of performance level loss data and recovery times. This implies that those models use system data and reflect the measurement in a single indicator. The most common resilience metrics use an idealized trajectory of system performance, where there is a decline in the performance of the system metric $X(t)$ drops after a disruptive event and increases over time. This is what is called as *resilience triangle* [6].

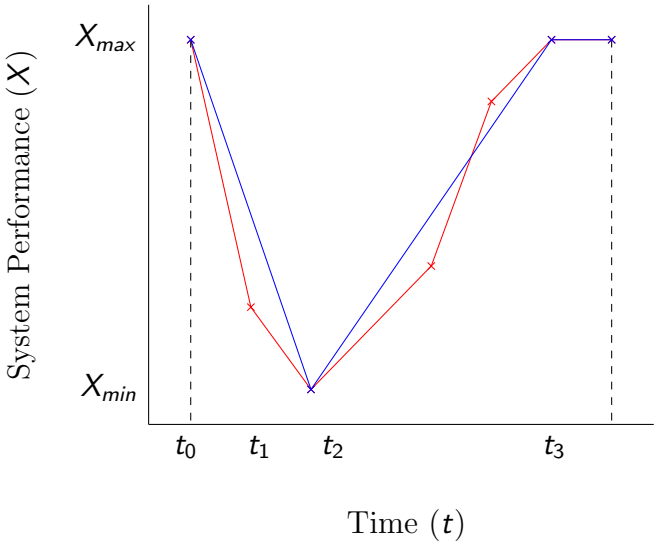

Figure 2.2: Representation of resilience triangle

Figure 2.2 shows in blue the *resilience triangle*, from which a metric is formulated. This metric considers the initial performance loss and recovery time to calculate the average performance of the system [7]. The metric related to the concept of the resilience triangle is considered one of the most commonly used metrics [9]. Theoretical estimation of the average

performance level is retrieved through the following equation:

$$R(t) = \frac{\int_{t_0}^{t_1}[1 - Q(t)]dt}{100(t_0 - t_1)}. \tag{2.1}$$

The function, $Q(t)$, quantifies the system's performances in percentage terms, t_0 is the time of the incident or disturbance occurrence, and t_1 is the time to full recovery [7]. The resilience units are performance per unit of time. This model quantifies the average performance of a relevant system outcome from when a disruptive event occurs until the system has fully recovered. A linear approximation of the average performance level was suggested by Zobel [6] to simplify the estimation and facilitate its practical applications.

$$R(t) = 1 - \frac{XT}{2T^*}. \tag{2.2}$$

In Equation 2.2, the parameter T denotes the total time that the system stays in a state of loss, i.e., the recovery time. X is the performance loss during the disruption [40]. Finally, T^* represents the control/monitored time and typically denotes the maximum recovery time. The system's resilience is 1 (or 100%) if either X or T equals 0 [16].

The idea of the average performance was extended by Ayyub[29] to the probabilistic scenario based on modeling disruption incidence as a Poisson process. This formulation considers three different time parameters: T_i (initial disruption time), ΔT_f (disruption duration), and ΔT_r (recovery time). In addition, F denotes the failure profile, and R is the recovery profile.

$$R = \frac{T_i + F\Delta T_f + R\Delta T_r}{T_i + \Delta T_f + \Delta T_r}. \tag{2.3}$$

Ayyub[29] describes the failure profile value F as a measure of robustness and redundancy (absorbing dimension). In contrast, the recovery profile value R can measure resourcefulness and rapidity (recovery dimension).

Finally, Romero & Savachkin [3] introduce the intensity-based resilience metric. This metric not only depends on the initial loss and the recovery time but adds the disruption intensity to the analysis, based on the idea that two systems that face two disruptions with different intensities and the same average performance should have different resilience levels.

$$R = \frac{I^2}{XT}. \tag{2.4}$$

In this case, I denotes the disruption intensity, X is the initial performance loss, and T is the recovery time. According to [3], this model facilitates the contrast of the resilience assessment in different system designs. Simultaneously the definition of the performance loss function, $X(I)$, and the recovery function, $T(X(I))$, enables a better understanding of a system's resilience for decision-making.

The above models are a sample of the wide variety of metrics available in the literature for resilience assessment. Unfortunately, they are also evidence of the lack of consensus on resilience definition [3]. However, there are some agreements on the dimensions that can characterize resilience, the absorbing dimension, and the recovery dimension [6]. The absorptive dimension is related to the system's robustness and capacity to mitigate initial loss posterior to a disruption. According to [7] the recovery dimension is the system's rapidity to recover and reach an acceptable level of functionality after a disruption.

In order to avoid issues regarding the lack of a formal resilience definition, this research presents a model based on resilience dimensions. The model considers parameters that, in a real-world context, are easy to monitor and track during the system's evolution within the recovery process, such as a system's performance level and recovery time.

Chapter 3: Research Objectives

The overall research objective is to develop stochastic models for dynamic resilience assessment and optimization.

These are the specific research objectives:

- Develop an optimization model for the dynamic allocation of resilience resources. The main objective is to minimize the cost of implementing actions that mitigate disruptions' impacts and reduce the recovery time. Then, a Continuous-Time Markov Decision Process (CTMDP) is provided to balance the intervention costs and enhance the long-run resilience assessment in a system.

- Research and identify testbeds for the optimization model's evaluation. The CTMDP model is applied in two testbeds considering different disruption scenarios: the Dique Canal breach in northern Colombia and a pandemic influenza outbreak via agent-based simulation. The optimal decision policies are retrieved for both testbeds and then assessed through Monte Carlo Markov Chain (MCMC) simulation.

Chapter 4: Continuous-Time Markov Decision Process Model Formulation

This section presents an infinite horizon discounted CTMDP model for the dynamic resource allocation during the post-disruption response of a physical system, where the objective is to minimize the total intervention costs and reduce the recovery time. We model the recovery as a continuous-time Markov process, where states transitions reflect the performance progress and sojourn times are exponentially distributed, as shown in Figure 4.1 [36, 13].

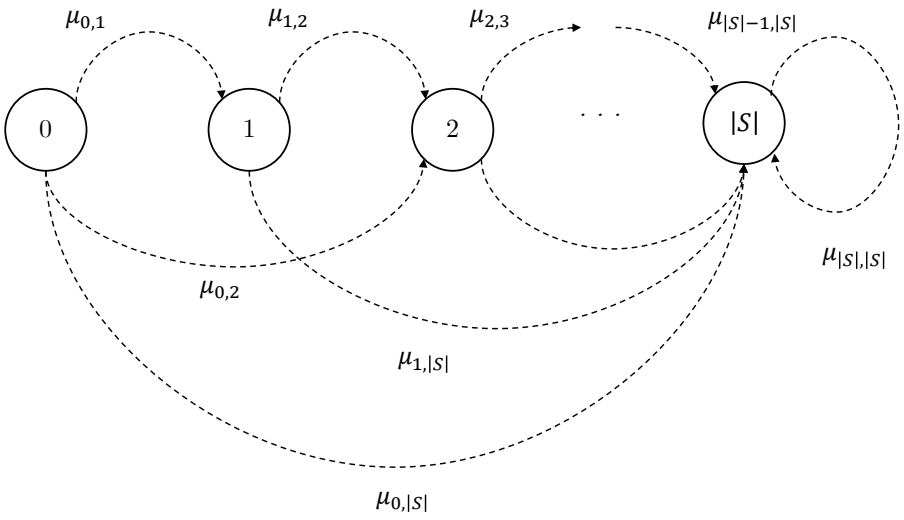

Figure 4.1: State transitions of the recovery process

In this formulation, we assume there is no intervention during the initial performance loss, so no mitigation actions nor backward transitions are considered, i.e., the system gradually returns to its pre-disruption conditions during the recovery process. In practice, not all disruptions reduce the performance of a system from its highest level to the lowest instantaneously. For instance, a mechanical system may have various stages of performance.

However, there is no gradual degradation in performance loss in physical systems such as infrastructure, depending on the type of disruptions, e.g., terrorist attacks or natural disasters. This behavior in the disruption modeling for resilience can be referred in [7, 40].

Figure 4.3 shows a summary schematic of our modeling framework, including state and action spaces, estimation of the state transition probabilities using uniformization, the cost function, optimality equations, and the stationary optimal recovery policy. In what follows, we present the details of each of these elements.

4.1 State Space

We consider a system which is monitored during the entirety of its recovery period $[0, T]$, following a disruption event. The system's relative performance levels are drawn from the the interval $[0, 1]$, where level 0 represents a totally dysfunctional system and level 1 corresponds to a normal condition. We partition the interval using n equally spaced recovery levels, marked $\{0, 1, 2, .., n-1\}$, from bottom-up, respectively. Let $X = \{0, 1, 2, .., n-1\}$ denotes the set of the recovery levels (see Figure 4.2).

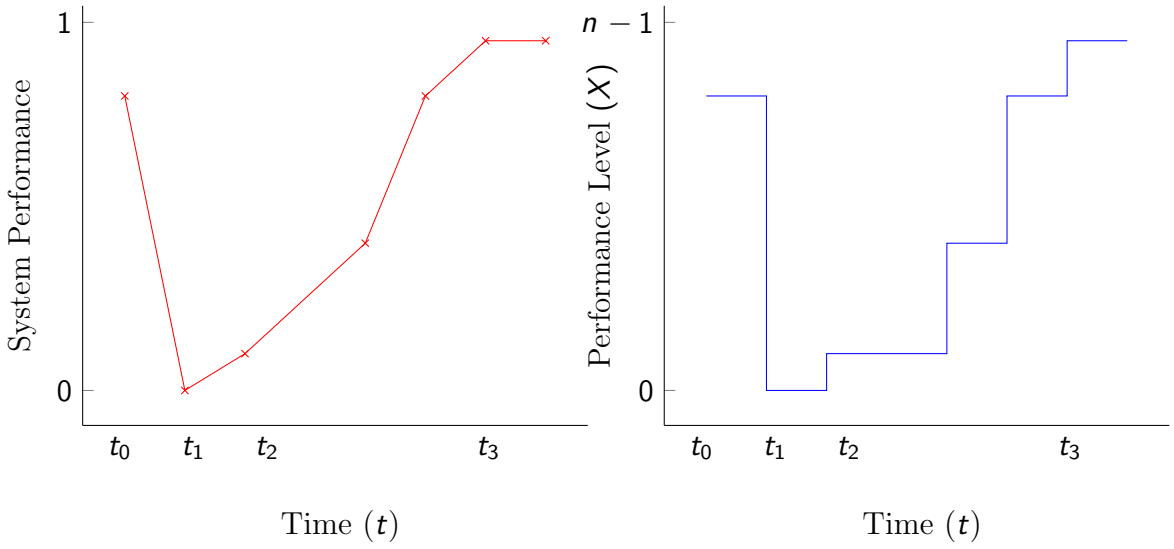

(a) Corresponding performance levels (b) System's relative performance $[0, 1]$

Figure 4.2: Representation of system's performance using a set of recovery levels

In a similar fashion, we partition the total available recovery budget as an ordered set of levels/sub-intervals $B = \{m-1, \ldots, 2, 1, 0\}$, where $m-1$ represents the highest budget interval, and 0 denotes the lowest one. Given the sets X and B, the system state space S is then defined as:

$$S = X \times B = \{(0, m), (0, m-1), ..., (n, 1), (n, 0)\}. \tag{4.1}$$

In addition, let i and j denote the current system state and the future system state, respectively, such that $i = (x, b)$ and $j = (x + \eta, b - \tau)$, for $\eta \in [0, n-1]$, $\tau \in [0, m-1]$, $x \in X$, $b \in B$, and $i, j \in S$.

4.2 Action Space and Generator Matrix

Let A_i denote the set of available actions in state i, where an action's cost is the cost of mitigation resources to be allocated to implement the action.

$$A_i = \{a_1, a_2, ..., a_K\} \text{ for } i \in S. \tag{4.2}$$

Let $a(i)$ denote the decision made in state i; this action can trigger a random transition out of the state after time Δt, based on transition rates $\mu_{ij}(a)$. The rates are assumed to be time-homogeneous, as in $Q(a) := [\mu_{ij}(a)]$ [46]:

$$Q(a) = \begin{bmatrix} -\sum_j \mu_{0,j} & \mu_{0,1} & \cdots & \mu_{0,|S|} \\ 0 & -\sum_j \mu_{1,j} & \cdots & \mu_{1,|S|} \\ \vdots & \vdots & \ddots & \vdots \\ 0 & 0 & \cdots & 0 \end{bmatrix} \tag{4.3}$$

From Equation 4.3, it is possible to observe that the system cannot return to a previous state once the recovery process starts.

4.3 Transition Probabilities

The time between transitions is exponentially distributed, so that $\Delta t \sim \exp(\mu_{ij}(a))$ [47]. As mentioned above, transitions between states depend on applying some action, and those transitions may occur from i to any j, implying that the system recovery process cannot go backward. Therefore, transitions may improve the current performance level and gradually recover all normal operative conditions.

There may be scenarios that involve multiple waves of the initial disruption or multiple disruptions from entirely different sources [23]. However, this formulation only focuses on recovery and does not consider those scenarios.

We built the Q-matrix in Equation 4.3 based on the previous considerations. From this matrix we estimate transition probability matrices $P(a)$ for each action $a \in A_i$, by applying the uniformization algorithm, as referred in [47, 48].

$$P(a) = I + \frac{1}{\gamma(a)} Q(a). \tag{4.4}$$

For Equation 4.4, $\gamma(a) \geq \max_{i \in S} |\mu_{ii}(a)|$, and represents the uniform rate parameter. So that, transition probabilities $p_{ij}(a)$ are estimated as follows:

$$p_{ij}(a) = \begin{cases} \dfrac{\mu_{ij}(a)}{\gamma(a)} & \text{for } i = j, \\ 1 - \dfrac{\sum_i \mu_{ij}(a)}{\gamma(a)} & \text{for } i \neq j. \end{cases} \tag{4.5}$$

Since the system will not return to a previous state, the probability for a backward transition is $p_{ji}(a) = 0$. However, when the system reaches an ideal/goal performance interval, $x = n - 1$, or the budget for recovery runs out, $b = 0$, in both cases, the system will be in

an absorbing state, i.e., $p_{ii}(a) = 1$. This indicates that the recovery process has ended or cannot continue because of the lack of resources.

4.4 Cost Function and Optimality Equations

Our expected cost function consists of two components. The first component is the setup cost $w(i, a)$, which is incurred by the system to implement action a in state i. It can include costs associated with resource planning, logistics setup, equipment setup, and similar costs. The second component of the function is the penalty cost for partial system functioning, which depends on the recovery cost rate $c(i, a)$ and the expected transition time. The cost rate is a parameter usually included in most CTMDP applications [47].

$$r(i, a) = w(i, a) + c(i, a)\mathbb{E}[\Delta t]. \tag{4.6}$$

On the other hand, a policy specifies the decision rule to be used at decision periods. It provides the decision-maker guidelines for action selection under any possible state. Since the objective is to minimize the total recovery cost finding an optimal policy depends on solving Bellman's optimality equations. Thus, we used the discounted model for CTMDP for defining and determining the optimal value function [47].

$$v^*(i) = \min_{a \in A(i)} \left\{ r(i, a) + \frac{\gamma(a)}{\gamma(a) + \lambda} \sum_{j \in S} p(j|i, a) v(j) \right\} \text{ for } i \in S. \tag{4.7}$$

$$a^*(i) = \arg \min_{a \in A(i)} \left\{ r(i, a) + \frac{\gamma(a)}{\gamma(a) + \lambda} \sum_{j \in S} p(j|i, a) v(j) \right\} \text{ for } i \in S. \tag{4.8}$$

Herein, $v^*(i)$ is the optimal expected cost of selecting an optimal action $a^*(i)$ in state $i \in S$. The optimal stationary recovery policy π^* is then a sequence of optimal actions taken in various states during the post-disruption response. Since the proposed methodology is based

on an infinite horizon CTMDP, the optimal recovery policy is stationary, and it is defined for the decision-maker as $\pi^* = (a^*)^\infty$.

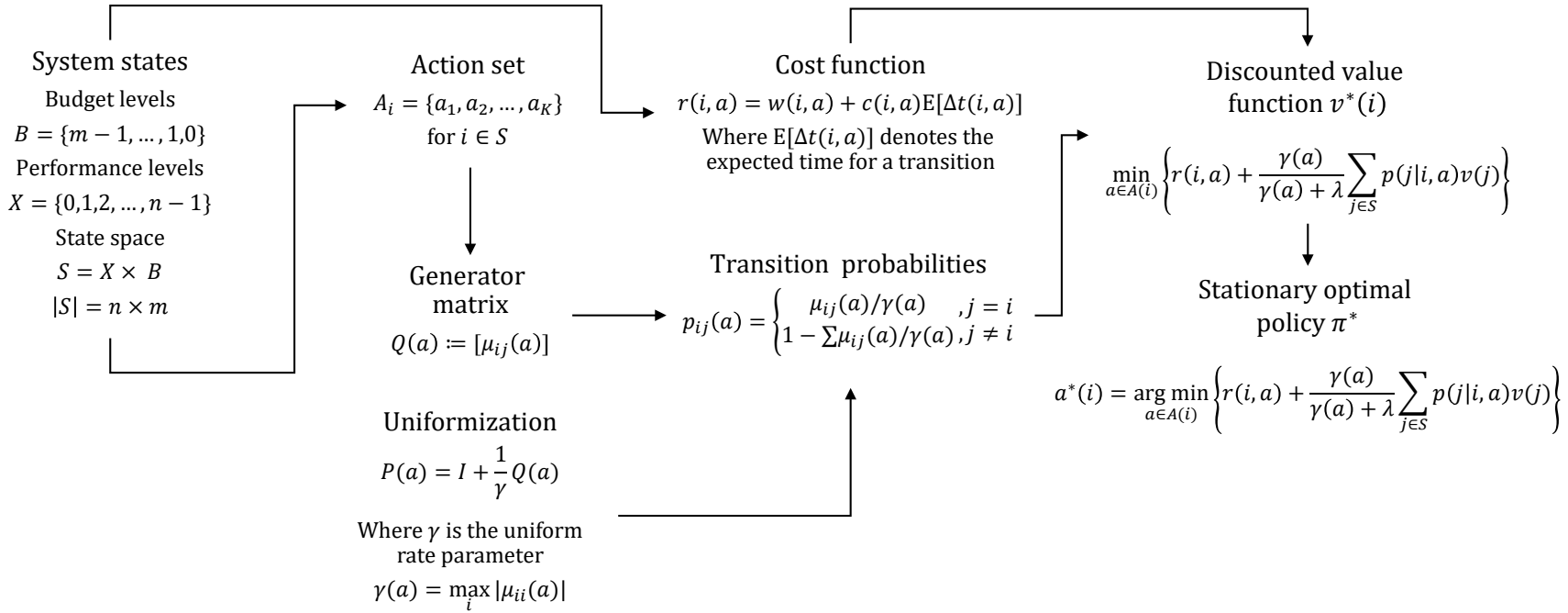

Figure 4.3: Schematic of the CTMDP model

Chapter 5: Study Case: Dique Canal Breach

5.1 Testbed Description

The resource allocation model is applied to a case study examining the economic impacts of the flood emergency in northern Colombia during the rainfall season in 2010. Due to its connection to Magdalena river (the longest river in Colombia), the Dique Canal has an annual cycle in which water levels can vary significantly between the dry (February through April) and rainfall (May through November) seasons. During the 2010 rainfalls, the water levels were extreme, reaching the overflow height in August with their maximum peaks between October and December.

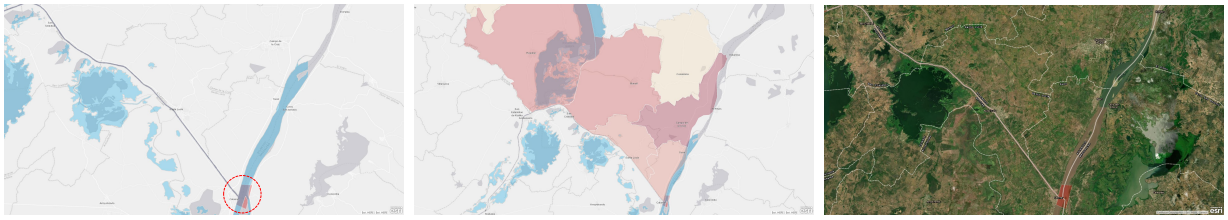

(a) Dique Canal location (b) Flooded area (c) Satellite view

Figure 5.1: Maps and satellite view of the flooded regions (produced by ArcGIS Online).

This unusual increase in the water levels resulted in a breach in one of the Canal's sections, followed by flooding of large community and agricultural areas between October and December. The disaster severely impacted five riverside towns: Suan, Campo de la Cruz, Santa Lucia, Manati, and Candelaria. The long-lasting consequences affected about 1.1 million people in these locations. Approximately 2.2 billion of cubic meters of water flooded the lowlands of the area damaging crops, cattle, and critical infrastructure. The total losses only in the agricultural sector were estimated in USD $180M [49].

Table 5.1: Timeline of the Dique Canal disaster, [1, 2]

Date	**Event**
30-Nov-10	Dique Canal breaches
13-Jan-11	80% of the flood water in Santa Lucia has receded
25-Jan-11	The breach is completely fixed
27-Jan-11	95% of the flood water in Santa Lucia has been removed
19-Feb-11	30% of the flood water in Campo de la Cruz has receded
14-Mar-11	82% of the flood water has receded
01-Jun-13	A plan to fully recover the canal is presented
Dec-18-20	Expected date for full recovery
Dec-20-20	Actual date of full recovery

Table 5.1 shows the timeline of the events after the rupture between Nov-2010 and Dec-2020.

5.2 Defining Performance and Budget Intervals

The testbed considers the expected post-disaster behavior of a physical system, where the initial performance loss is almost instantaneous, and no intervention action is implemented to mitigate it. We used the habitability index to quantify the recovery of the flooded area and determine the system's state in the recovery process. Habitability is a complex concept related to the notion of quality of life and integrates six social aspects (health, housing, accessibility, education, economy, and environment)[50]. To estimate the habitability index, we use the approach suggested in [1], where it is calculated as the percentage of the available area for normal living conditions in each rural town based on floodwater levels and necessary infrastructure availability.

For this testbed, we used six nominal intervals of the habitability index based on different recovery stages, ranging between 0% (no habitability remained) and 100% (full recovery), as shown in Table 5.2. During the performance levels $x = 0$ and $x = 1$, intervention strategies focus on the initial emergency response. The practical difference between both of them is the expected costs and time needed to reach full recovery from any of them. We considered the

same situation for performance levels $x = 2$ and $x = 3$, where recovery actions are mainly focused on infrastructure restoration.

Table 5.2: System performance (habitability index) levels

X	**Habitability (performance) intervals**	**Recovery stages**	**Description**
0	(0, 0.1)	Post-disruption initial stage	Lowest performance level
1	(0.10, 0.25)	Initial emergency response	Water removal, humanitarian attention, debris clearance, temporary housing plan, food supply
2	(0.25,0.40)	Infrastructure & housing restoration (Phase I)	Critical infrastructure (highways, primary and secondary roads) housing relocations, and installation of temporary hospitals
3	(0.40,0.65)	Infrastructure & housing restoration (Phase II)	Housing financial support, healthcare services reactivation, education services reactivation
4	(0.65, 0.85)	Economic & business reactivation	Economic support infrastructure (secondary roads, warehouses, logistic infrastructure), business support services, healthcare, and education continuity
5	(0.85, 1)	Community preparedness	Risk management and disaster prevention. Non-critical infrastructure restoration

To determine the budget levels set B, we used data from several official sources, including government institutions and private organizations [49, 2], which estimated that between \$147M and \$225M were collected as the recovery fund for the region. We partitioned the total fund (budget) using ten equally spaced levels, $B = \{9, 8, ..., 1, 0\}$.

The state space was then taken as $S = \{(0, 9), (0, 8), \ldots, (5, 1), (5, 0)\}$, and $|S| = 60$.

5.3 Intervention Actions and Costs

Given the actual response-recovery duration from November 2010 through December 2020 (see Table 5.1, the planning horizon T was taken to be 10 years for this testbed. For this total period, five nominal intervention/action strategies were considered: short-term (labeled as a_0), short-medium (a_1), medium (a_2), long-medium (a_3), and long-term (a_4). For each element of the action space $A = \{a_0, a_1, a_2, a_3, a_4\}$, the respective expected time to full

recovery was assumed to be 36, 48, 60, 90, and 120 months, from the moment of engaging the strategy and assuming that the strategy remains the same until a complete recovery.

A policy is a rule that maps a system state to an intervention strategy. For our testbed, an example of a policy is using the short-term strategy during the initial recovery to prioritize emergency relief for the primary response (water removal, humanitarian logistics, debris clearance, etc.). Once the initial phase is complete, depending on the system state, the policy can shift to the medium or long-medium-term strategy for infrastructure intervention and economic reactivation.

Table 5.3: Dique canal tesbed: actions costs

Performance levels X	**Action costs ($ Millions)**					**Disruption loss cost rate ($ Millions/month)**
	Short (a_0)	**Medium-short** (a_1)	**Medium** (a_2)	**Medium-long** (a_3)	**Long** (a_4)	
0	72.79	63.97	59.55	57.35	55.14	0.70
1	60.66	53.31	49.63	47.79	45.95	0.59
2	48.53	42.64	39.70	38.23	36.76	0.47
3	36.39	31.98	29.78	28.67	27.57	0.35
4	24.26	21.32	19.85	19.12	18.38	0.23

Table 5.3 shows the costs of the actions as a function of the system state. The values were estimated from publicly available economic data, government reports, journal articles, and news stories [49]. For any action/state combination, the corresponding cost is bound by the available budget, which limits the possible actions at a decision maker's disposal at that state. The table also shows the estimates of the average economic monthly losses by being in each of the recovery states (e.g., agricultural loss from the flooding of the croplands, livestock maintenance cost, etc. [49]).

5.4 Numerical Results

This section shows the results for our testbed, starting with the optimal recovery policy for the CTMDP model. The policy's performance is then assessed using a discrete event sim-

ulation. The results will be analyzed and insights provided, focusing on the model outcomes and system's resilience assessment.

5.4.1 Optimal Stationary Policy

We used the value iteration algorithm to obtain the optimal stationary CTMDP policy using a precision constant of 10^{-30} and a discount rate α of 5×10^{-5}. Table 5.4 shows the optimal decision for each possible state, i.e., for each pair of the combination between performance and budget level. For instance, for a performance level of $x = 0$ and budget level of $b = 9$ the optimal decision is a_1, which is a medium-short term action with a implementation cost equals to \$63.97M.

Table 5.4: Optimal stationary policy for the Dique canal area recovery

Budget levels (B)	**Performance levels (X)**									
	0		1		2		3		4	
	action	cost	action	cost	action	cost	action	cost	action	cost
9	a_1	63.97	a_0	60.66	a_1	42.64	a_1	31.98	a_3	19.12
8	a_1	63.97	a_1	53.31	a_1	42.64	a_1	31.98	a_3	19.12
7	a_1	63.97	a_1	53.31	a_1	42.64	a_2	29.78	a_3	19.12
6	a_1	63.97	a_1	53.31	a_1	42.64	a_2	29.78	a_3	19.12
5	a_1	63.97	a_1	53.31	a_2	39.7	a_3	28.67	a_3	19.12
4	a_1	63.97	a_1	53.31	a_2	39.7	a_3	28.67	a_3	19.12
3	a_2	59.55	a_3	47.79	a_3	38.23	a_3	28.67	a_3	19.12
2	a_2	59.55	a_3	47.79	a_3	38.23	a_3	28.67	a_3	19.12
1	a_2	59.55	a_3	47.79	a_3	38.23	a_3	28.67	a_3	19.12
0	a_3	57.35	a_3	47.79	a_3	38.23	a_3	28.67	a_3	19.12
action costs units: \$ in Millions										

As it can be seen from the table, in general, the policy calls for a medium-short term intervention in the early stages of the recovery process when the budget allows it. Such an approach allocates a relatively large amount of resources during the primary response for immediate emergency relief. The response then subsides to medium and long-medium-term actions (infrastructure intervention and economic reactivation). The policy avoids long

interstate transitions trying to balance the intervention costs and the recovery time. In addition, the policy does not indicate any action when the system is in any state where $x = 5$. At that point, the system reaches its pre-disaster level, so the recovery process ends, and no action is longer needed.

5.4.2 Simulation and Policy Performance Evaluation

We used a MCMC to assess the performance of the optimal recovery policy. We considered a 95% confidence level and a permissible error of 1.5% to calculate the sample sizes, i.e, the total number of iterations. The sufficient number of replications for estimating the mean recovery time and mean recovery cost were 6,305 and 2,365, respectively. Since the computational times were relatively low, we implemented 100,000 iterations. Figure 5.2 shows system's recovery patterns for three runs.

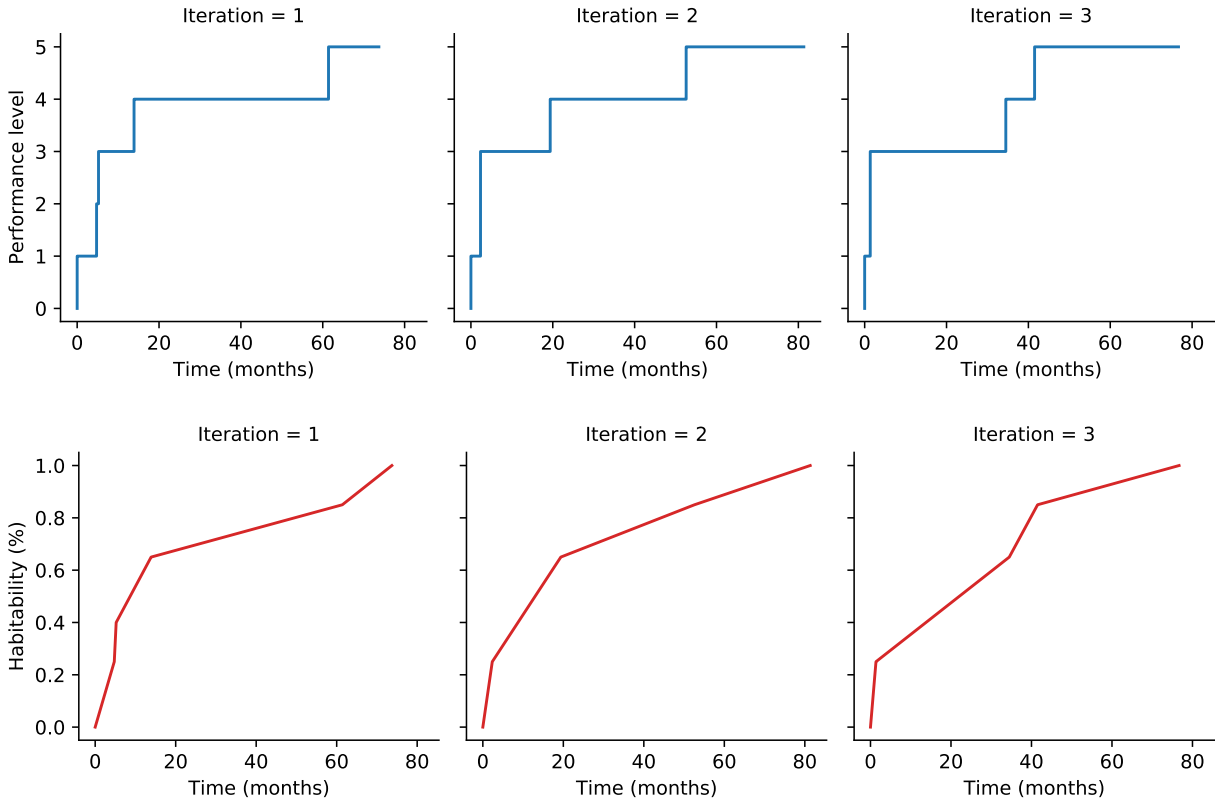

Figure 5.2: MCM Simulation sample for optimal recovery policy

Table 5.5 shows simulation statistics for the optimal policy compared to two alternative policies: fastest (which selects short-term actions in all states) and lowest-cost (which selects long-term actions in all states). The three policies are listed from the highest to the lowest mean recovery time. In addition, we also compared the mean recovery costs, the budget utilization, and the average resilience of these policies. Further details on resilience assessment are presented in Section 5.4.3.

Table 5.5: Dique canal testbed: summary of results

Policies	**Recovery time (months)**			**Recovery costs ($ in Millions)**			**Budget utilization (%)**	**Average resilience - Zobel (%)**
	Mean time	95% Lower bound	95% Upper bound	Mean cost	95% Lower bound	95% Upper bound		
Fastest	35.96	35.81	36.10	185.98	185.65	186.32	70.02	84.95
OptimaL	71.17	70.87	71.47	181.26	180.90	181.60	59.41	70.51
Low-cost	120.25	119.77	120.74	211.04	210.58	211.50	53.80	49.96

The results show that under the optimal policy, the system returns to its pre-disaster habitability level between 70 to 72 months, with an average cost of about $181M. As expected, the mean recovery time for the optimal policy (70 months) is higher than the fastest (36 months) but lower than the lowest-cost policy (120 months). Thus, the fastest policy has a better performance in terms of resilience. However, since the objective was to balance the intervention costs in the system, the optimal policy is the one that ensures the minimum costs and a reasonable resilience level of 70.51%, only 16% lower than the fastest policy. Furthermore, the average budget utilization for the fastest policy is 18% higher than the optimal policy, implying that the cost of implementing actions is lower for the optimal policy.

The optimal policy also has significant advantages over the government intervention in the Dique Canal breach. The actual restoration of the communities in the impacted region took around 120 months to complete, and a total investment between $147M and $225M

[1, 49, 2]. The optimal policy cuts the recovery time by around 40%, based on the budget utilization, and reduces the restoration investment to approximately $133M, almost by 10%.

Figures 5.3 and 5.4 show histograms and box plots of the recovery times and recovery costs for simulations of the three policies.

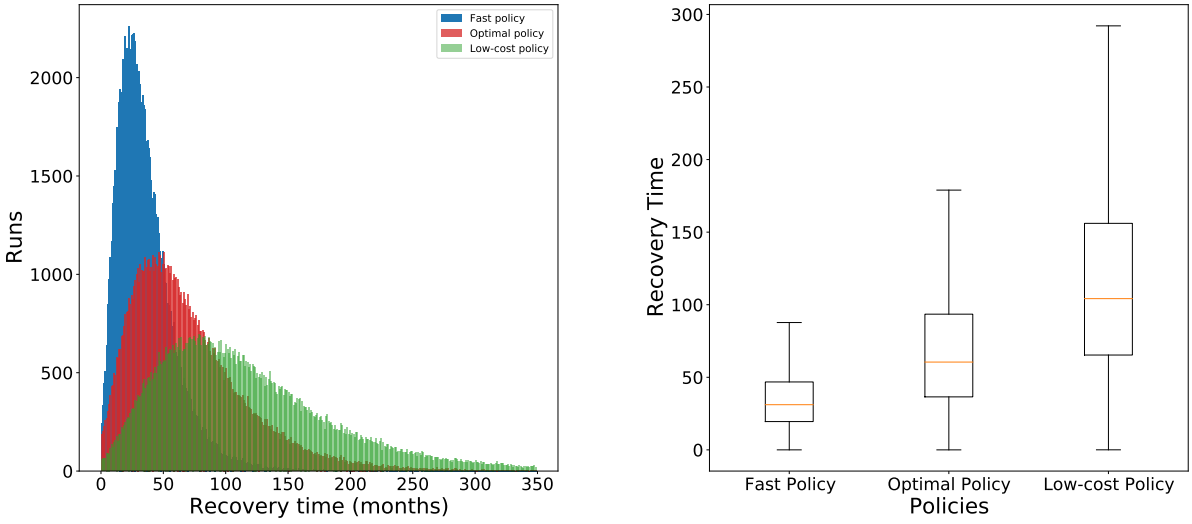

(a) (b)

Figure 5.3: Recovery times comparison

Table 5.6: ANOVA results for recovery policies (times and costs comparison)

	Source of variation	*df*	Sum of squares	Mean square	*f*	*p*-value	*f*-critic
Time	Policies	2	2.27×10^7	1.13×10^7	3641	2×10^{-16}	2.99
	Residuals	18912	5.88×10^7	3110.45			
	Total	18914	8.15×10^7				
Cost	Policies	2	1.23×10^6	6.16×10^5	156.3	2×10^{-16}	2.99
	Residuals	7092	2.79×10^7	3941			
	Total	7094	2.92×10^7				

We carried out a single-factor ANOVA for the recovery time and the cost to determine if the difference in the performance for the three policies is statistically significant. Results

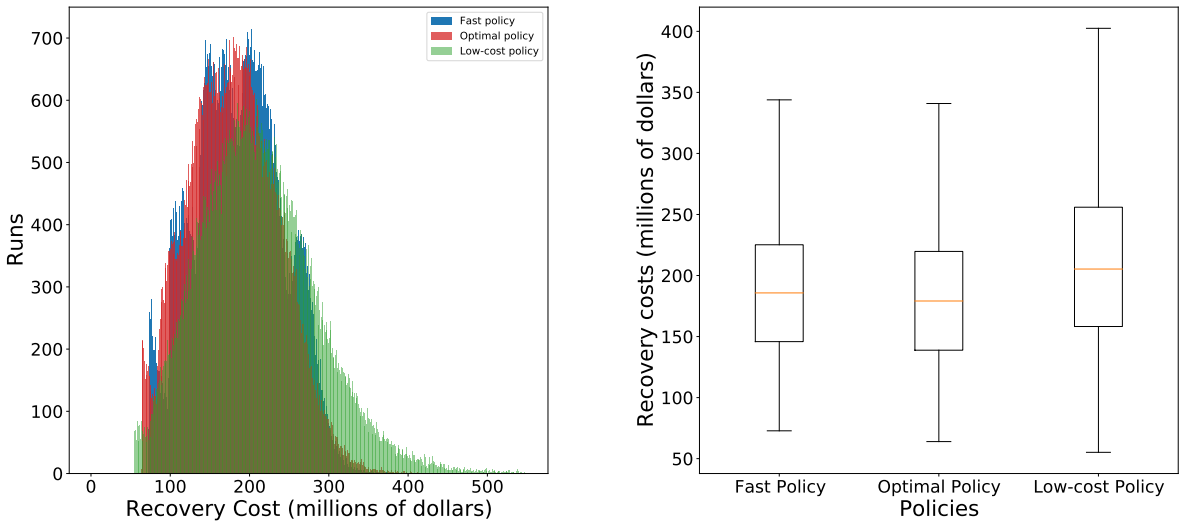

(a) (b)

Figure 5.4: Recovery costs comparison

are shown in Table 5.6. In addition, we used a t-test for paired policies with a confidence level of 95% for each combination to obtain further insights (Table 5.7).

Table 5.7: T-test results for recovery policies (times and costs comparison)

	Policy comparison	t	p-**value (two-tail)**	t-**critical (two-tail)**
Times	Fastest vs. Optimal	-50.550	0.0	1.960
	Fastest vs. Low-cost	-80.209	0.0	1.960
	Optimal vs. Low-cost	-42.262	0.0	1.960
Costs	Fastest vs. Optimal	2.792	0.005	1.960
	Fastest vs. Low-cost	-13.257	0.0	1.960
	Optimal vs. Low-cost	-15.443	0.0	1.960

Expectedly, the fastest policy has the best recovery time, but it also has the highest budget utilization. The low-cost policy is the worst in terms of time and cost due to the penalty for long transition times. The optimal policy shows the lowest cost with a decent recovery time and a budget utilization close to the lowest-cost policy. In addition, we consider

the resilience assessment as part of the policy performance evaluation. However, we will discuss further details in the following subsection.

5.4.3 Resilience Assessment

This section shows a resilience based comparison of the three recovery policies. There are a number of resilience metrics in the literature Generally, they try to capture the dynamics of a system's performance level, as the system recovers from a disruption back to normalcy. In our analysis, we used a *resilience triangle* type of measure introduced by Zobel [6], which uses a linear approximation of the average performance level to facilitate both the estimation of resilience and practical applications of resilience based design. According to the metric, the system's resilience at time t is given as:

$$R = 1 - \frac{XT}{2T^*}, \tag{5.1}$$

where T is the total recovery time, X is the initial drop in performance, and T^* is the control time (planning horizon).

In our assessment of resilience for the three policies based on Equation 5.1, we used 100% of performance loss (based on the records of public reports [49]) and considered a range of time between 60 and 120 months for T^*.

Table 5.8: Mean resilience comparison for recovery policies

T^*	**Fastest policy**			**Optimal policy**			**Long-term policy**		
	95% Lower bound	Mean resilience	95% Upper bound	95% Lower bound	Mean resilience	95$ Upper bound	95% Lower bound	Mean resilience	95% Upper bound
60	72.93	73.04	73.15	46.5	46.72	46.95	9.72	10.09	10.45
75	78.35	78.43	78.52	57.2	57.38	57.56	27.78	28.07	28.36
90	81.96	82.03	82.1	64.33	64.48	64.63	39.82	40.06	40.3
105	84.53	84.6	84.66	69.43	69.56	69.69	48.41	48.62	48.83
120	86.47	86.52	86.58	73.25	73.36	73.48	54.86	55.05	55.23
Planning horizon (T^*) in months									

The results are listed in Table 5.8. Since the metric is a function of time, lower recovery times imply higher resilience. In this case, the fastest policy has the highest resilience but also highest recovery costs and budget utilization. In our model, we tried to find a balance between resilience and its cost. In that sense, the optimal policy minimizes the recovery cost and attains a reasonable resilience level (as compared to that of the fastest policy).

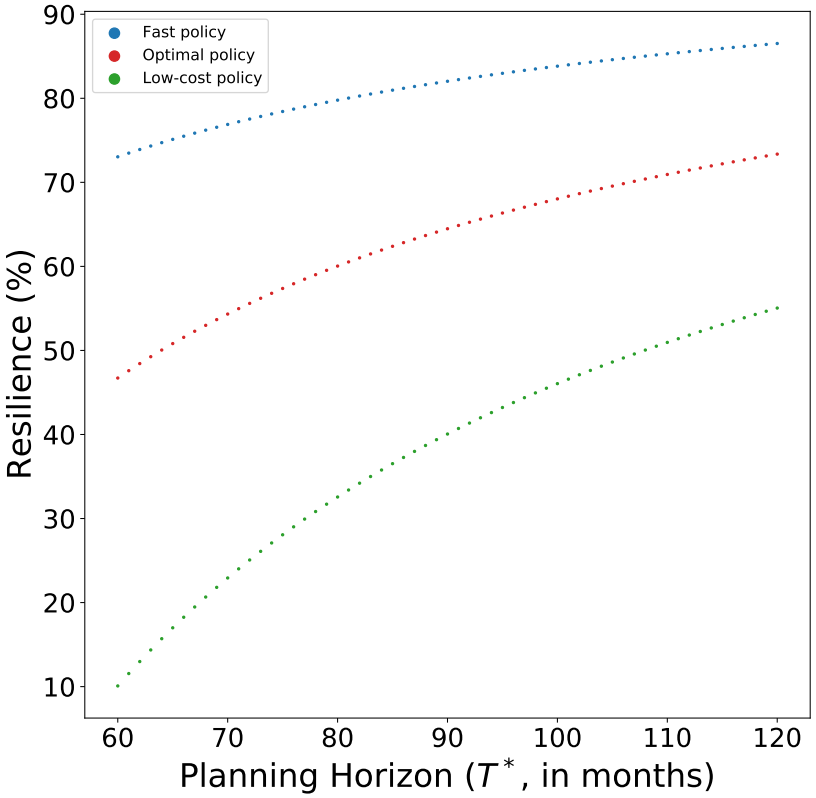

Figure 5.5: Average resilience comparison for recovery policies

Figure 5.5 shows the dynamics of resilience over time for the three policies. The optimal policy was again in-between the fastest and long-term policies. It can also be noted that as recovery progresses, the rate of resilience gain is higher for the optimal policy than for the fastest policy, which implies that the system can reach its normalcy relatively faster.

5.4.4 Recovery Probabilities Distribution

Some authors have used the distribution of recovery time T (known as recovery probabilities) as a metric for resilience quantification under uncertain conditions [29, 51, 52]. In this section, we compare the three recovery policies using such a metric. Since our CTMDP model assumed independent and exponentially distributed sojourn times, we expected T to follow a gamma distribution. We applied the maximum likelihood method to find the point estimators of the distribution's shape (Equation 5.2) and scale parameters (Equation 5.3) for each of the policies [53]

$$\alpha = \frac{1}{2\log\sum_i^N \frac{T_i}{N} - 2\sum_i^N \frac{\log T_i}{N}} \tag{5.2}$$

$$\beta = \frac{1}{\alpha N}\sum_i^N T_i, \tag{5.3}$$

where N is the sample size (total number of simulation runs) and T_i is the recovery time of simulation i.

Table 5.9: Estimated values of α and β parameters of T_i distributions and recovery probabilities

Policies	**Parameters**		**Probabilities**				
	α	β	$P(T < 36)$	$P(T < 48)$	$P(T < 60)$	$P(T < 90)$	$P(T < 120)$
Fastest	2.243	16.073	0.589	0.749	0.853	0.966	0.993
Optimal	2.003	35.395	0.270	0.393	0.505	0.721	0.852
Long-term	2.249	53.495	0.103	0.169	0.242	0.427	0.588
			T (time in months)				

Figure 5.6 shows schematics of the estimated T distributions for three recovery policies (see Table 5.9 for distribution parameter values as well as the estimated values of the recovery probabilities for a number of time intervals for the three policies). From the table and the picture, it is highly probable that implementing either the fastest or, to a lesser extent, the

optimal policy can fully recover the system within 120 months. The marginal rate of increase in the recovery probability during the initial phases is noticeably higher for the fastest policy, which then reaches a saturation at about 80 months into the recovery. Notwithstanding its higher budget utilization, the fastest policy could be a better choice, if a rapid recovery in short term is the goal.

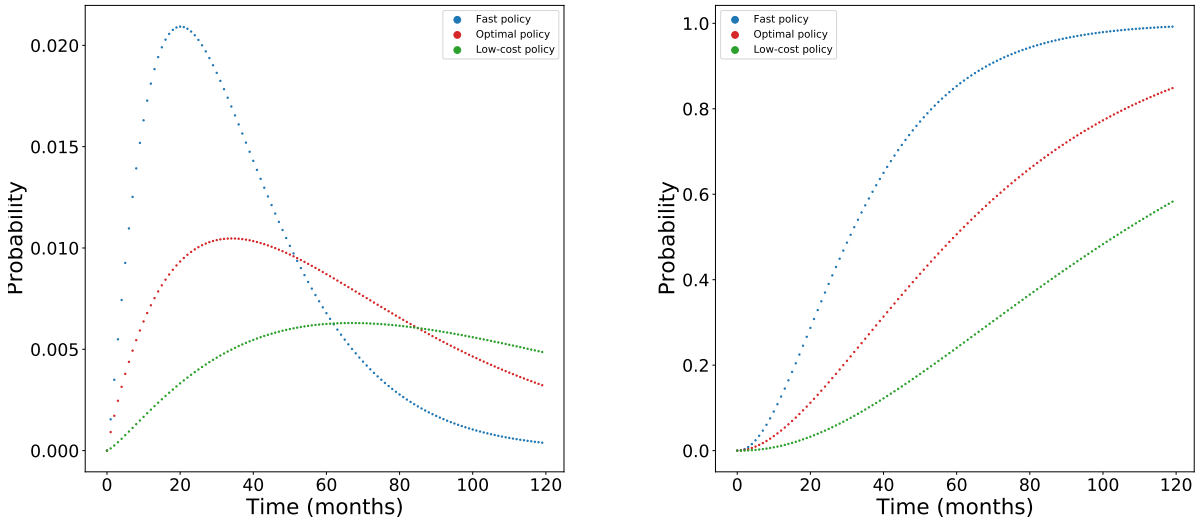

(a) Probability density functions

(b) Cumulative distribution functions

Figure 5.6: Recovery probabilities comparison

Since both policies emphasize allocating resources during the early stages of the recovery process, in practice, an expedited primary response is essential to a rapid increase in the recovery probabilities. At the same time, even though late recovery stages are essential to returning to pre-disruption conditions, moderate amounts of resources during the infrastructure intervention and economic reactivation can enable attaining high recovery probabilities within 120 months. This outcome can be explained by the emphasis both policies put on emergency relief during the early stages of the recovery process.

Additionally, we also remark that even though late recovery stages are essential to return to the pre-disruption conditions, relatively moderate amounts of allocated resources during

the infrastructure intervention and economic reactivation facilitate high recovery probabilities. This approach on the decision-making is relevant if we consider that implementing medium and long-medium-term actions is necessary to balance total intervention costs.

Chapter 6: Study Case: Pandemic Outbreak Mitigation

6.1 Mitigation Oriented Model

In a pandemic outbreak, mitigation strategies aim to reduce the social impacts (e.g., deaths by infection), avoid the collapse of healthcare facilities, and prevent the disruption of essential services. The most prudent approach is to expand medical capacity as much as possible while lowering the expected healthcare service demand by limiting virus spread. Postponing a rapid upswing of cases and reducing the infected peak would allow a better match between the number of ill individuals requiring hospitalization and a community's capacity to provide medical care for those individuals (see Figure 6.1) [54].

Nevertheless, it's improbable that the most effective tool for mitigating a pandemic (i.e., a well-matched pandemic strain vaccine) will be available. So, non-pharmaceutical interventions (NPIs) may help to reduce virus transmission by reducing contact between sick and uninfected individuals, thereby reducing the number of infected cases. Non-pharmaceutical interventions typically include social distancing, isolation, lockdowns (workplaces/schools closures), and travel restrictions [54].

This focus on reducing potential losses increases the system's absorptive capacity and enhances its resilience. However, implementing aggressive NPI actions produces significant economic impacts in the communities [12]. For instance, through the recent COVID-19 crisis, the implementation of lockdown measures involved decrements in the international economic growth [8]. In the USA, projections of GDP impacts exceed those for the Great Recession, with losses ranging between $3.2 and $5 trillion [55]. In developing countries like Colombia, preventive isolation measures aggravated the vulnerability conditions for the population, where the poverty levels increased from 1.5 to 4.4 million people [56, 57].

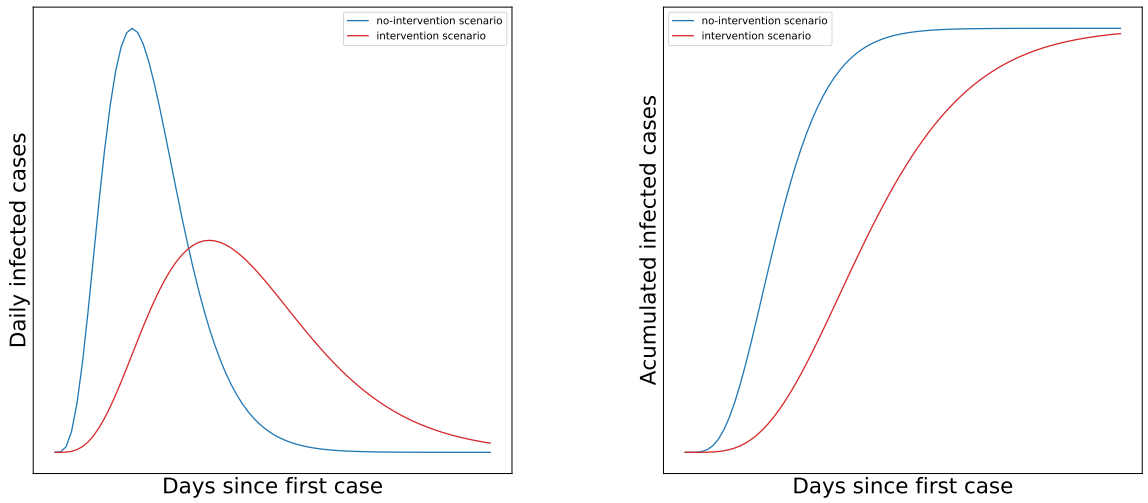

(a) Daily infected cases distribution

(b) Cumulative infected cases distribution

Figure 6.1: Delaying outbreak peak

NPI's economic effects involved negative consequences on the quality of life of individuals in a community. So, our primary goal with this pandemic testbed is to mitigate social and economic impacts by lessening the number of infected and balancing the intervention costs. We do so by implementing some adjustments into our MDP model.

Figure 6.2 shows the new summary schematic of our modeling framework under a pandemic mitigation scenario. Changes in the state space, generator matrix, and cost function are proposed to fit the model to the above considerations. In what follows, we present further details of these adjustments.

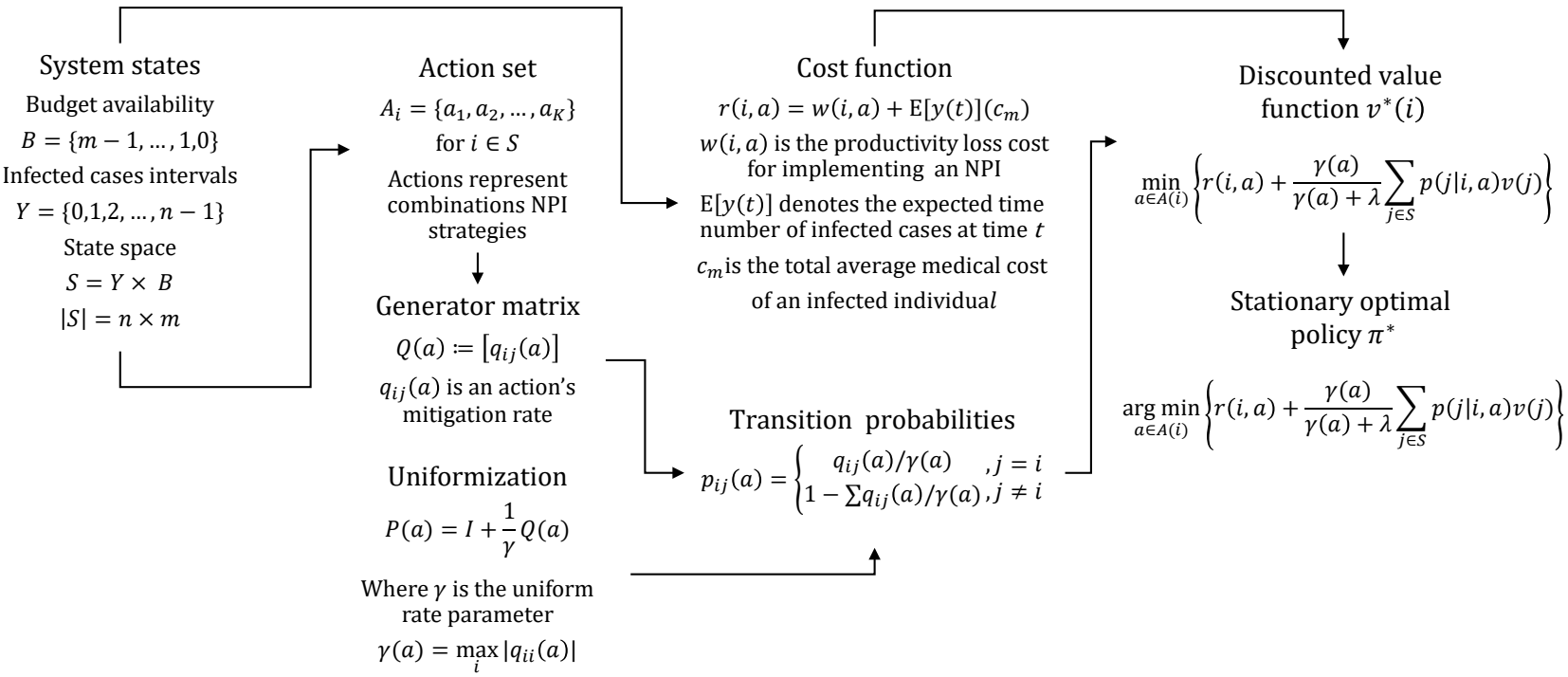

Figure 6.2: Schematic of the CTMDP model for pandemic mitigation.

6.1.1 State Space for Pandemic Mitigation

We consider a community monitored within the time interval $[0, T]$ during a pandemic outbreak. Decisions are made at the end of the time interval $[0, t]$, where t represents the accumulative time until the next decision and $0 \leq t \leq T$.

Additionally, we referred to the traditional SIR model for pandemic dynamics for our state space definition [58], where a large population of N individuals and a disease in which infection spreads by contact between individuals. Each individual is susceptible, infectious, or recovered at any time. Once a susceptible person becomes infected, they eventually die, are isolated, or recover and become immune. Thus, at any time, the population is comprised of a proportion $x(t)$ of susceptible individuals, a proportion $y(t)$ of infected and circulating individuals, and a proportion $z(t)$ of individuals who either have been removed (by death or isolation) or are immune. Therefore,

$$x(t) + y(t) + z(t) = 1 \text{ for } t \in [0, T]. \tag{6.1}$$

Since the main goal is to delay a rapid upswing of infected cases and lower the epidemic peak, the current model focuses on the proportion of infected individuals $y(t)$. This proportion is taken to be the interval $[0, L]$, where 0 represents the total lack of infected individuals and L is the final proportion of infected individuals, and $L \in (0, 1]$. We replicate the approach we used in the Dique Canal testbed and partition the interval using n infected individuals levels, marked $\{0, 1, 2, .., n-1\}$, from the bottom-up, respectively. Let $Y = \{0, 1, 2, \ldots, n-1\}$ denote the set of infected cases levels within the $[0, T]$ interval.

In our pandemic testbed, we considered the following set of percentage infected cases intervals $\{(0, 0.05), (0.05, 0.1), (0.1, 0.25), (0.25, 0.65), (0.65, 100)\}$, and set $Y = \{0, 1, 2, 3, 4\}$. To determine the set of budget levels B, we assumed a large enough budget for the entire mitigation process. Similarly to our procedure in the previous chapter, we partitioned the total fund using ten equally spaced levels, $B = \{9, 8, \ldots, 1, 0\}$.

The state space was then taken as $S = \{(0,9),(0,8),...,(4,1),(4,0)\}$, so $|S| = 50$.

6.1.2 Transition Rates for Pandemic Mitigation

In this pandemic mitigation testbed we consider the proportion of individual infected cases as a performance metric to track the community response during a virus propagation. This proportion of individuals may rise or lessen depending on the pandemic's dynamics over time. Furthermore, multiple waves with peaks in the number of infected individuals are typically expected in a pandemic outbreak [59]. Figure 6.3 illustrates a multiple waves pandemic scenario.

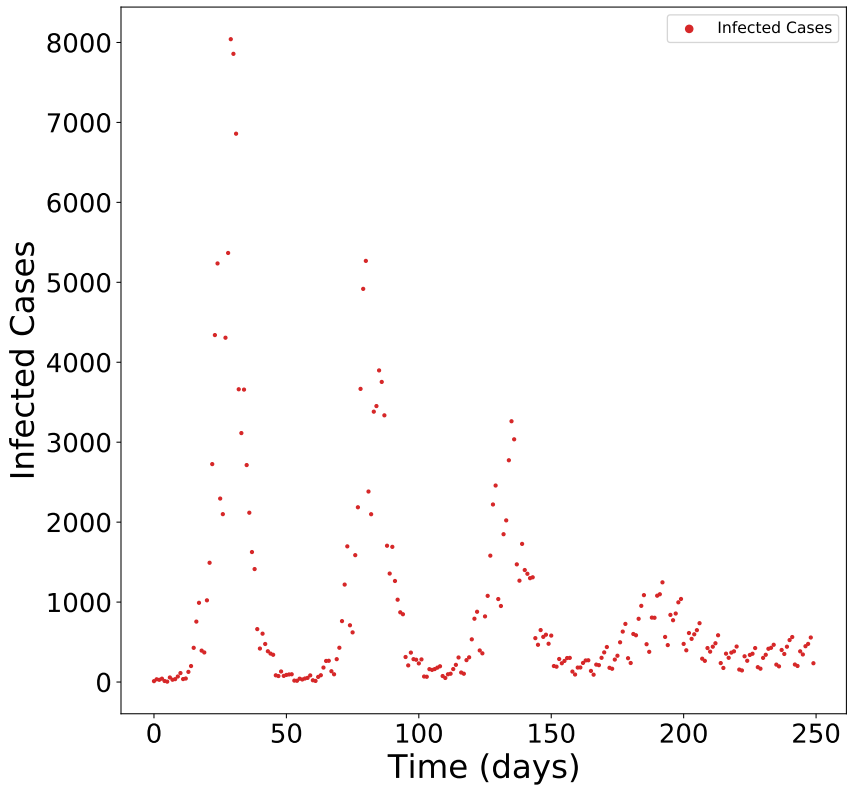

Figure 6.3: Multiple waves pandemic outbreak

The CTMDP model can capture the above behavior by allowing forward and backward transitions between the states. We expand the rate transition matrices and consider mitigation rates for all possible transitions (see Equation 6.2).

$$Q(a) = \begin{bmatrix} -\sum_j q_{0,j} & q_{0,1} & \cdots & q_{0,|S|} \\ q_{1,0} & -\sum_j q_{1,j} & \cdots & q_{1,|S|} \\ \vdots & \vdots & \ddots & \vdots \\ q_{|S|,0} & q_{|S|,1} & \cdots & -\sum_j q_{|S|,j} \end{bmatrix} \tag{6.2}$$

From Equation 6.2, it is possible to observe that the system can return to a previous state once the mitigation process starts. In addition, mitigation rates are not time functions, so the Q-matrix for the model is time-homogeneous.

6.1.3 Cost Function for Pandemic Mitigation

The pandemic mitigation costs function resembles the costs function for the Dique Canal testbed. In this case, we also consider two cost components. The first component is the setup cost, which represents the economic impacts of implementing an NPI action. For instance, it can include costs associated with mandatory quarantines or the closure of workplaces and schools. The second component is the cost of keeping infected individuals in the population. This cost can include the cost of medical treatment and healthcare services and the death toll costs.

$$r(i, a) = w(i, a) + c_m(i, a)\mathbb{E}[y(t)]. \tag{6.3}$$

In Equation 6.3, $w(i, a)$ represents the setup cost, $c_m(i, a)$ is the medical treatment cost rate per infected individual, and $\mathbb{E}[y(t)]$ is the expected number of infected cases at time t. Notice that for our testbed, we only focus on the infected individuals, so we do not include any penalties for deaths in the model.

6.2 Testbed Description

For the pandemic testbed, we used the latest version of the agent-based (AB) simulation model developed in preceding studies of influenza pandemics by [17, 5, 18]. This simulation model reproduces an influenza pandemic outbreak in a population of 1.2 million individuals. In addition, the model deems epidemiological parameters, including the incubation and latent period, demographic information, infection process, contact process, and disease's natural history. Figure 6.4 shows the schematic of the AB simulation model.

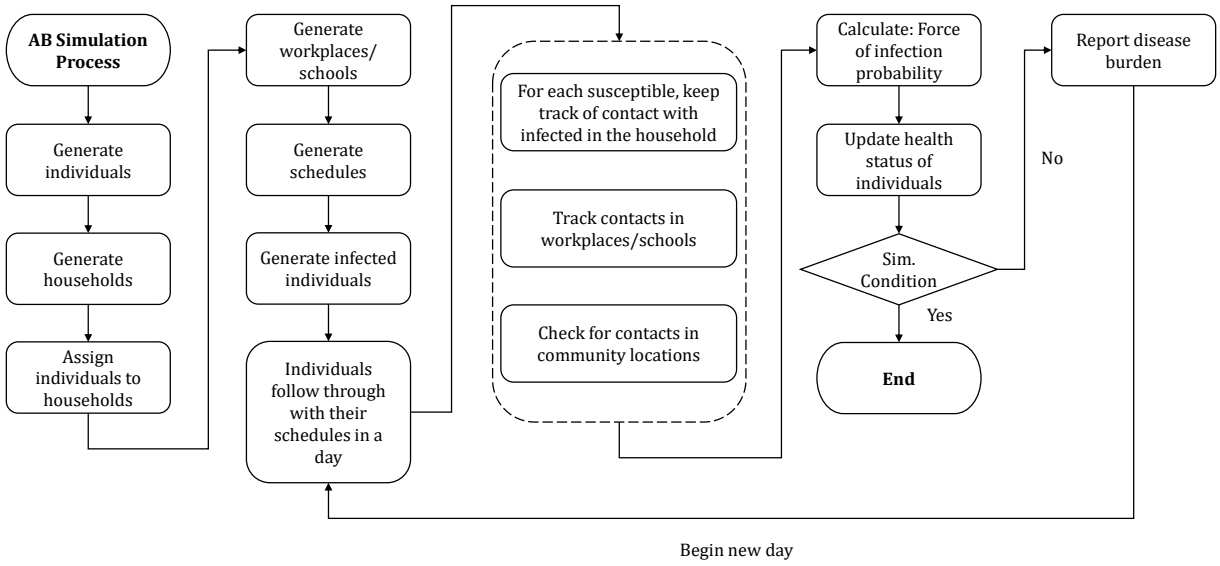

Figure 6.4: AB simulation model schematics [5, 4]

The simulation model generates individuals and their households in an outbreak region. Afterward, the model assigns schools, workplaces, and communities and the daily activity schedule appropriate for different types of individuals. An outbreak is triggered when the model releases infected individuals in the population, and then it keeps track of the daily status of each person. Susceptible individuals become infected depending upon the force

of the infection [17, 5, 4]. Then, the infected follow the disease's natural course and either recover and become immune or die.

We ran the AB model and tested 30 combinations of non-pharmaceutical interventions, including isolation, household quarantine, and school and workplace closure. Table 6.1 displays the parameter generator functions. Parameters' values are not modified once we generate them for a single simulation run. For all the combinations, we deemed the same disease propagation scenario, i.e., the force of the infection.

The output summary file for each simulation model run contains relevant information on intervention costs and pandemic dynamics, e.g., the number of infected, recovered, and deceased individuals. In our testbed, we used the number of infected patients in each state as input to estimate the transition rates and build the transition rate matrices for all NPI combinations. In addition, we also used the data from the summary file to estimate the parameters for the mitigation cost function.

6.3 Numerical Results

This section presents the results of the pandemic tested. Where we replicated the structure, we followed in Chapter 5, starting with the optimal mitigation policy for the CTMDP model. Then, the policy's performance is assessed via discrete event simulation. Finally, the results will be analyzed, and insights provided, focusing on the policy's performance and the system's resilience assessment.

6.3.1 Optimal Stationary Policy

We again implemented the value iteration algorithm to retrieve the optimal stationary policy. For this testbed, we considered a constant of 10^{-2} and a discount rate α of 10^{-5}. Table 6.2 shows the optimal decision for each of the states (infected cases level and budget level). On the other hand, Table 6.3 shows a detailed description of each one NPIs in the optimal policy. For instance, for the infected cases level $y = 0$ and budget level $b = 9$, the

Table 6.1: NPIs generator functions [3, 4]

Non-Pharmaceutical Interventions (NPIs)	**Description**	**Parameters**
Global threshold	Number of cases needed to declare an outbreak of influenza	10
Deployment delay	Time necessary to fully deploy NPIs	Uniform (3,7)
Case isolation period	Time that an infected individual should stay at home	Uniform (7,10)
Case isolation compliance for workers	Compliance rate for workers	Uniform (0.53,0.75)
Case isolation compliance for non-workers	Compliance rate for non-workers	Uniform (0.57,0.84)
Household quarantine period	Time that a household member is restricted to move	Uniform (7,10)
Household compliance of workers	Compliance rate for workers' households	Uniform (0.53,0.75)
Household compliance of non-workers	Compliance rate for non-workers' households	Uniform (0.57,0.84)
Cases to close a class in a school	Number of infected students in a class to close the class	Uniform (1,3)
Classes to close a school	Number of closed classes to close a school	Uniform (1,3)
School closure period	Time that a school remains closed	Uniform (14,42)
Cases to close a department in a workplace	Number of workers in a department to close the department	Uniform (3,5)
(%) of departments to close a workplace	Percentage of closed departments to close a school	Uniform (0.3,0.6)
Workplace closure duration	Time that a workplace remains closed	Uniform (7,14)

optimal decision a_7 calls for a combination of NPI which considers an isolation period of 7 days, 14, and 7 days of schools and workplaces closure, respectively.

As seen from Tables 6.2 and 6.3, in general, NPIs combinations in the optimal policy consider isolation periods between 7 and 14 days and schools and workplaces' closures periods between 7 and 21 days. The policy tends to be more moderate in the early stages of

Table 6.2: Optimal stationary policy for pandemic outbreak mitigation

Budget Levels (B)	**Infected Cases Levels (Y)**									
	0		1		2		3		4	
	NPI	cost	NPI	cost	NPI	cost	NPI	cost	NPI	cost
9	a_3	1.10	a_4	0.86	a_{29}	173.63	a_{14}	681.67	a_{27}	408.85
8	a_3	1.10	a_4	0.86	a_{29}	173.63	a_{14}	681.67	a_{27}	408.85
7	a_3	1.10	a_3	2.23	a_{29}	173.63	a_{14}	681.67	a_{27}	408.85
6	a_3	1.10	a_3	2.23	a_{29}	173.63	a_{14}	681.67	a_{27}	408.85
5	a_3	1.10	a_3	2.23	a_{29}	173.63	a_{14}	681.67	a_{27}	408.85
4	a_3	1.10	a_3	2.23	a_{29}	173.63	a_{14}	681.67	a_{27}	408.85
3	a_3	1.10	a_3	2.23	a_{29}	173.63	a_{14}	681.67	a_{27}	408.85
2	a_3	1.10	a_7	1.11	a_{29}	173.63	a_{14}	681.67	a_{27}	408.85
1	a_3	1.10	a_7	1.11	a_{29}	173.63	a_{14}	681.67	a_{27}	408.85
0	a_7	1.28	a_7	1.11	a_{29}	173.63	a_{10}	581.65	a_{27}	408.85
all costs are in $ millions										

the pandemic outbreak, suggesting isolation periods of 7 days and school closure duration between 14 and 21 days. Afterward, especially in the high and mid-levels of the infected number, the policy became more aggressive by doubling the isolation period and fixing the schools' closure up to 21 days.

Additionally, since triggers for activating quarantine and closure measures show the policy's sensitivity level, they are essential for establishing its effectiveness against virus propagation. For instance, at the beginning of the mitigation process, the percentage of departments for a workplace closure is between 40% and 60%. Then, the interval falls between 30% and 50% in the late stages. Such an approach implies the policy is balancing the costs of the isolation measures for workplace closures and the social impacts (medical treatment costs and deaths) of virus propagation. This emphasis on reducing the economic effects on the population is also noticeable when the policy recommends the lowest possible period (7 days) for workplace closures in most cases.

Table 6.3: NPIs combinations in the optimal policy for pandemic mitigation

NPIs	**Parameters Combinations**						
	a_3	a_4	a_7	a_{10}	a_{14}	a_{27}	a_{29}
Global threshold	10	10	10	10	10	10	10
Deployment delay	7 days	7 days	3 days	7 days	3 days	7 days	3 days
Case isolation threshold	1 days	1 days	1 days	1 days	1 days	1 days	1 days
Case isolation period	7 days	14 days	7 days	7 days	7 days	14 days	14 days
Case isolation compliance for workers	68%	64%	53%	72%	60%	67%	70%
Case isolation compliance for non workers	75%	73%	64%	63%	75%	74%	77%
Household quarantine threshold	1 days	1 days	1 days	1 days	1 days	1 days	1 days
Household quarantine period	8 days	8 days	8 days	7 days	9 days	10 days	8 days
Household compliance of workers	62%	63%	75%	72%	71%	72%	73%
Household compliance of non workers	64%	57%	79%	64%	72%	57%	58%
Cases to close a class in a school	2	2	1	3	3	1	3
Classes to close a school	1	1	3	3	3	1	1
School closure period	21 days	21 days	14 days	14 days	14 days	21 days	14 days
Cases to close a department in a workplace	5	5	5	5	5	5	5
(%) of departments to close a workplace	40%	50%	60%	50%	50%	40%	30%
Workplace closure duration	7 days	7 days	7 days	14 days	7 days	7 days	7 days

6.3.2 Policy Simulation and Performance Assessment

We used an MCMC simulation to assess the performance of the optimal mitigation policy before the population reaches a cumulative proportion of 15% of infected cases. We considered a 95% confidence level and a permissible error of 1.5% to calculate the sample sizes (total number of iterations). The necessary number of iterations for estimating the mean time and mitigation cost were 10,490 and 27,834, respectively. However, we implemented 50,000 iterations since the computational times were relatively low. Figure 6.5 shows the pandemic mitigation patterns for three sample runs.

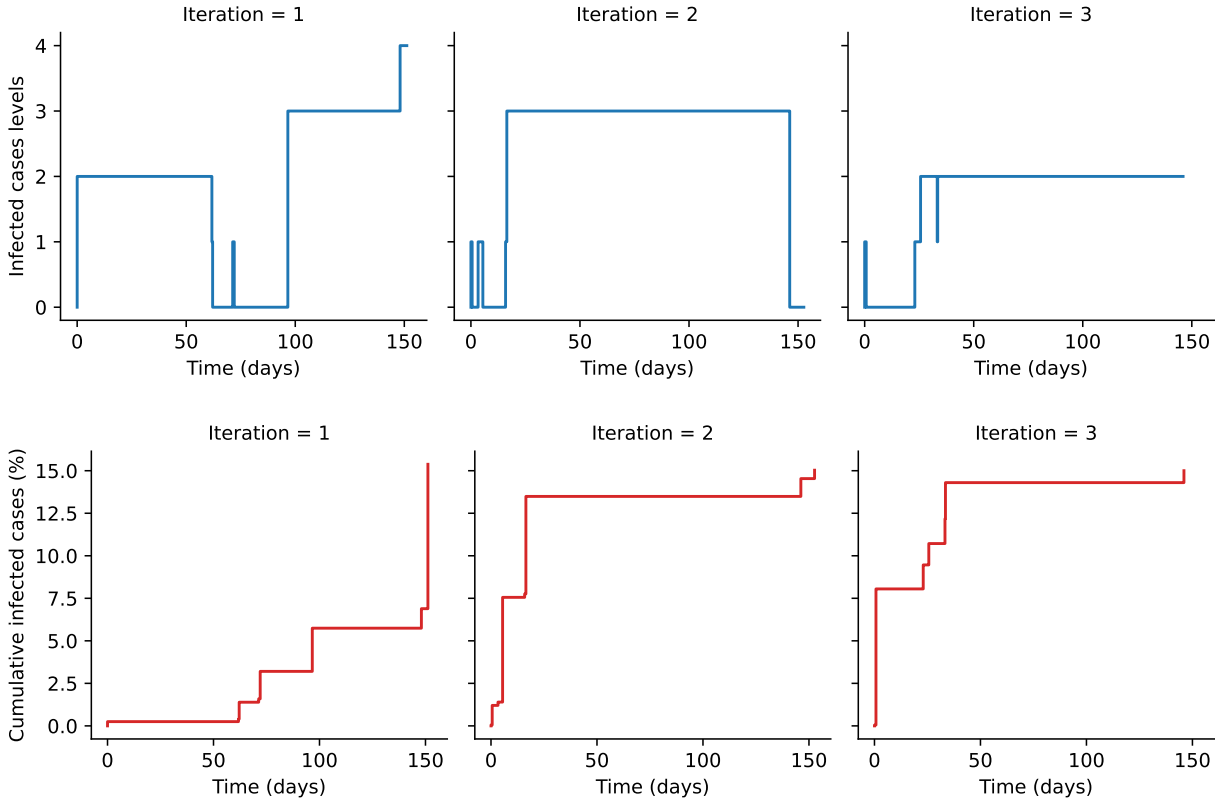

Figure 6.5: MCMC Simulation sample for optimal pandemic mitigation policy

Table 6.4 shows the simulation statistics summary for the optimal policy compared to the baseline scenario (no intervention) and three alternative mitigation policies:

- Min-time: selects the actions with the shortest expected transition times.

- Max-time: selects the actions with the longest expected transition times.

- Max-cost: selects the combination of actions that maximizes the mitigation costs.

We focused our analysis on two parameters, the time to reach 15% of total infected individuals and mitigation costs. The results of the resilience assessment comparison are presented in Section 6.3.3.

Table 6.4: Pandemic testbed: summary of results

Policies	**Propagation Times (days)**			**Mitigation Costs ($ hundred of millions)**		
	Mean Times	95% Lower bound	95% Upper bound	Mean Costs	95% Lower bound	95% Upper bound
Optimal	145.32	144.13	146.51	4.14	4.09	4.20
Min-Time	142.22	141.08	143.36	13.85	13.76	13.94
Max-Time	170.41	169.26	171.55	141.42	140.59	142.25
Max-Cost	209.08	207.71	210.44	154.96	154.08	155.84
Base-Line	119.75	118.82	120.68	25.17	24.99	25.35
Propagation times for up to 15% of population infected cases						

The results from Table 6.4 show that under the optimal policy, the proportion of cumulative infected individuals reaches 15% after 145-146 days of the first contagion, with a total average mitigation cost of about $414 M. Notice that higher propagation times imply a reduction in the number of infected individuals. As expected, the max-time and max-cost policies were more effective in delaying virus propagation, with mean times 42% and 75%, respectively, higher than the baseline scenario, while the optimal and the min-time policies had a relatively good performance, 21% and 19%higher than the baseline scenario. However, since the main objective was to minimize the intervention cost, the optimal policy yielded the minimum mitigation cost, which was 84% lower than the baseline and 97% lower than the max-cost policy.

Figures 6.6 and 6.7 show histograms and box plots of the virus spread times and mitigation costs for all simulated scenarios.

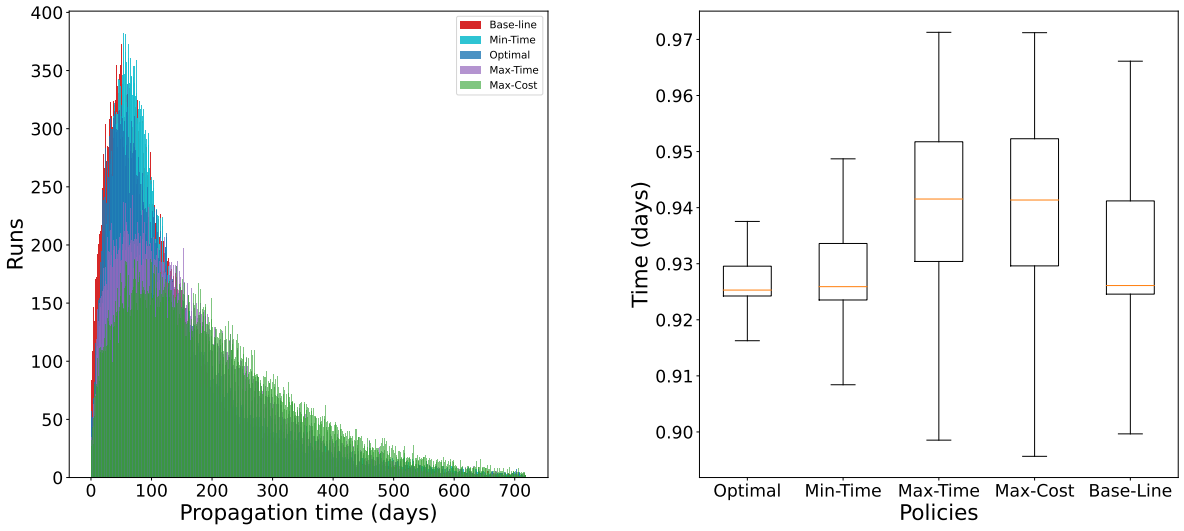

(a) (b)

Figure 6.6: Virus propagation times comparison

We carried out a single-factor ANOVA for the virus propagation times and the mitigation costs to determine if the difference in the performance for all simulated scenarios is statistically significant. Results are shown in Table 6.5.

Table 6.5: ANOVA for mitigation policies (times and costs comparison)

	Source of variation	*df*	**Sum of squares**	**Mean square**	*f*	***p*-value**	***f*-critic**
Time	Policies	4	2.20×10^8	5.49×10^7	3641	2×10^{-16}	2.99
	Residuals	237500	4.18×10^9	17597			
	Total	237504	4.40×10^9				
Cost	Policies	2	1.23×10^6	6.16×10^5	156.3	2×10^{-16}	2.99
	Residuals	7092	2.79×10^7	3941			
	Total	7094	2.92×10^7				

Results do not differ from our expectations. The max-cost and max-time policies are the most effective in reducing virus propagation, but they also have the most significant economic impacts on the system. On the other hand, the min-time policy performs similarly

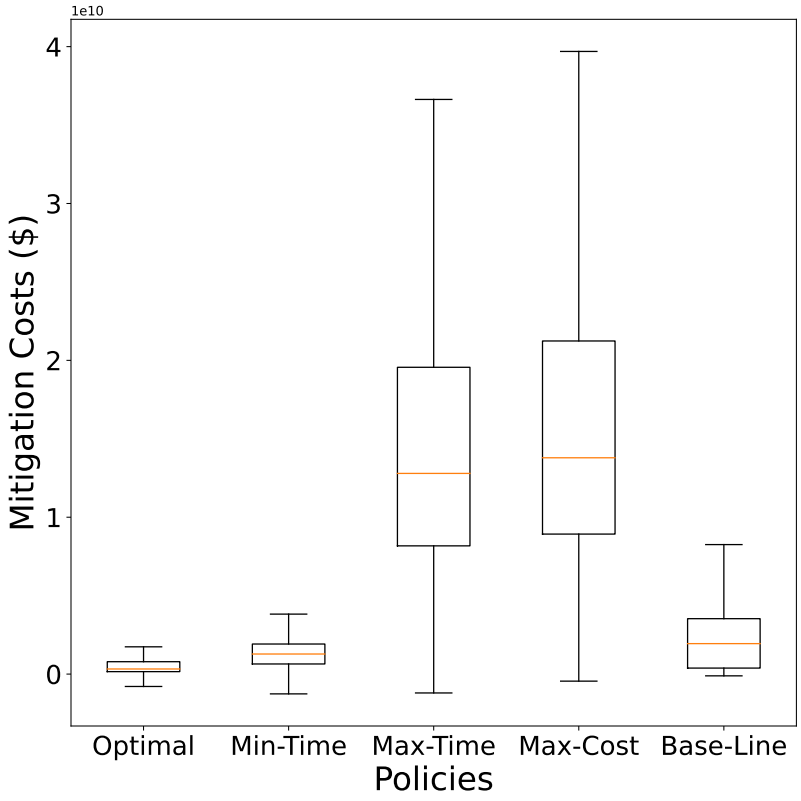

Figure 6.7: Pandemic mitigation costs comparison

to the optimal policy but has relatively considerable economic effects. Overall, the four policies involve improving the system response against the virus spread at different levels. Still, the optimal policy minimizes the costs for the pandemic mitigation and significantly reduces the economic impacts on the system.

6.3.3 Resilience Assessment

This subsection presents a resilience-based comparison of all the scenarios examined in the above section (Section 6.3.2). In the resilience assessment, we used the measure introduced in [4] for resilience and preparedness during pandemic outbreaks. This metric quantifies resilience levels through the average performance and cumulative loss functions. In addition, it easily incorporates into the simulation model to be implemented.

The metric considers the fraction of the healthy population over time, $H(t)$, as the critical performance variable to quantify the community response during the virus propagation.

$$H(t) = H(t-1) - \frac{Y(t) + Rec(t)}{N - \int_0^T D(t)} \tag{6.4}$$

In Equation 6.4, $Y(t)$ represents the number of infected individuals at time t. Likewise, $Rec(t)$ represents the number of recovered, and $D(t)$ is the number of deaths due to the virus at time t, respectively. Finally, N denotes the initial population size, and parameter T is the number of days since the beginning of the outbreak.

$$R = \int_{T_{OE}}^{T_{OE}+T_{LC}} \frac{H(t)}{T_{LC}} dt \tag{6.5}$$

Equation 6.5 shows the global resilience metric for pandemic disruption scenarios. The parameter T_{OE} is the starting moment of the outbreak, and T_{LC} corresponds to the control time. Typically, this time is greater or equal to the recovery time, and the decision-maker defines it. Nevertheless, in the context of our testbed, T_{LC} represents the expected time to reach 15% of infected individuals from the population since it is the control time for MCMC simulation. This metric ranges between 0 and 1 and indicates how well the system withstands the disruption.

Table 6.6: Mean resilience comparison for mitigation policies

Policies	**Resilience Statistics**				
	Mean	Standard Deviation	CV	95% Lower bound	95% Upper bound
Optimal	85.86	2.52	0.029	85.83	85.88
Min-Time	86.05	2.64	0.031	86.02	86.07
Max-Time	88.10	2.95	0.033	88.07	86.12
Max-Cost	88.05	3.10	0.035	88.02	88.07
Base-Line	86.36	2.86	0.033	86.34	86.39
Resilience values in (%)					

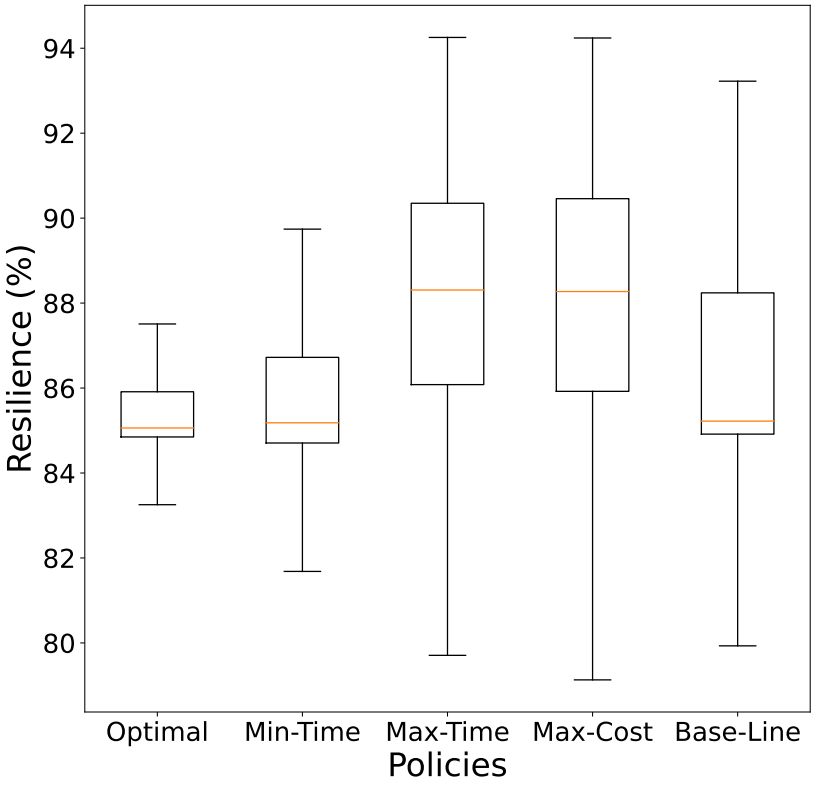

Figure 6.8: Average resilience comparison for mitigation policies

Figure 6.8 shows statistically significant differences between the four policies and the baseline scenario results. However, Table 6.6 shows that those differences from a practical perspective are not considerable. Notice that the confidence intervals are extremely close and nearly overlap.

In general, the mean resilience for all tested scenarios is between 85% and 88%. This result is an expected outcome since the cumulative number of infected does not overpass 15% of the total individuals in the population. In this case, the resilience metric captures the system's absorptive capacity for all the scenarios, so the resilience assessment reflects the performance loss during the early stages of the pandemic outbreak. This loss is reflected in the number of infected individuals.

6.3.4 Virus Propagation Probabilities

In this subsection, we replicate our approach to determine the recovery probabilities for the Dique Canal testbed. However, the emphasis is on the virus spread during the MCMC simulation control time in this case. Since our CTMDP model still assumes independent and exponentially distributed sojourn/transition times, times for virus propagation, T_i, are expected to follow a gamma distribution. Once again, we applied the maximum likelihood method to find the point estimators of the distribution's shape and scale parameters for all simulated scenarios. Results are listed in the Table 6.7.

Table 6.7: Estimated values α and β parameters of T_i distributions and virus propagation probabilities

Policies	**Parameters**		**Probabilities**				
	α	β	$P(T > 30)$	$P(T > 60)$	$P(T > 90)$	$P(T > 120)$	$P(T > 180)$
Optimal	1.28	113.89	0.86	0.71	0.58	0.46	0.29
Min-Time	1.49	95.19	0.89	0.74	0.59	0.47	0.28
Max-Time	1.50	113.32	0.91	0.79	0.66	0.55	0.37
Max-Cost	1.55	134.78	0.94	0.84	0.74	0.64	0.46
Base-Line	1.37	87.63	0.84	0.66	0.51	0.39	0.21
			T (time in days)				

Figure 6.9 shows schematics of the estimated T_i distributions for the four policies and the baseline scenario.

Probabilities analysis provides insights regarding the policies' effectiveness to retard the virus spread in the population. For instance, the marginal rate of increase in the probability curve during the initial phases is noticeably lower for the max-cost policy, which then reaches saturation at about 135 days into the pandemic mitigation process. Notwithstanding its higher economic impacts, the max-cost policy could be a better choice if minimizing the virus propagation were the objective.

Overall, all policies provide preferable scenarios compared to the baseline. However, the optimal policy shows a reasonable effectiveness level against virus propagation despite

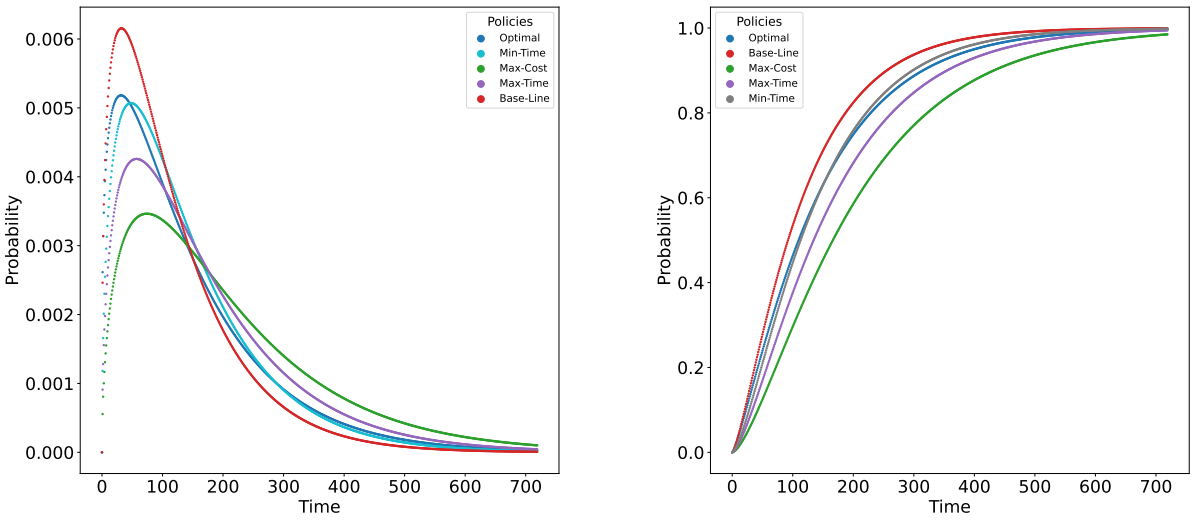

(a) Probability density functions

(b) Cumulative distribution functions

Figure 6.9: Virus propagation probabilities comparison

its moderate approach to suggesting isolation and closure periods. Hence we can state the optimal policy performs relatively nicely while minimizing the community's economic impacts.

Chapter 7: Conclusions

This dissertation's main goal is to provide a decision support model for the post-disruption resource allocation to balance the costs of resilience. We employed a stochastic dynamic approach, more precisely a CTMDP formulation, since the post-disaster response can be analyzed as a random process. The proposed model considers a bivariate state space based on the system's performance and available budget, resources to allocate in a particular decision period, and exponentially distributed transition times.

7.1 Summary of Results

The model's primary outcome is the optimal stationary policy, i.e., the optimal sequence of actions (resources to allocate) for all decision periods. We used the value iteration algorithm to derive the optimal stationary policy for two testbed scenarios: the Dique Canal rupture in northern Colombia and a pandemic influenza outbreak via agent-based simulation. We also assessed the policies' performance via simulation and focused our analysis on key parameters: recovery and virus propagation times, mitigation costs, average budget utilization, and average resilience.

In the Dique Canal testbed, we compared the optimal policy versus two other policies, the fastest policy (ensures minimal recovery time) and the lowest-cost policy (ensures minimal budget utilization). Afterward, we found that the mean recovery time for the optimal policy is around 97% higher than the fastest policy and 69% lower than the lowest-cost policy. The recovery cost gap among the three policies is not very large; the optimal policy is 2% lower than the fastest policy and 16% lower than the lowest-cost policy. However, the average

budget utilization for the fastest policy is 18% higher than the optimal policy, which implies that the cost of implementing actions is lower for the optimal policy.

In the pandemic testbed we compared the optimal policy versus the baseline scenario (no intervention) and three alternative policies: the min-time policy (ensures the shortest transition times), the max-time policy (guarantees the slowest transition times), and the max-cost (maximizes the mitigation costs). Results showed that under the optimal policy, the proportion of total infected individuals in the population goes to 15% after 145-146 days from the beginning of the outbreak, with a total average mitigation cost of about $414 M. As expected, the optimal policy minimized the economic impacts on the system. The mitigation cost for the optimal policy was 84% lower than the baseline and 97% lower than the max-cost policy.

Simulation enabled us to generate data to identify the recovery and propagation times distributions. Since the total times are the summation of exponentially independent transition times, recovery and propagation times for both testbeds fit a gamma distribution.

7.2 Key Findings

The implementation of both testbeds suggests significant insights. In the Dique Canal case, the optimal recovery policy calls for an intensive intervention in the early recovery stages, allocating a relatively large amount of resilience resources during the primary response for emergency relief. At the same time, medium and long-medium-term actions play a significant role in balancing total recovery costs during the infrastructure intervention and economic reactivation phases. A proper cost function is essential in attaining an equilibrium between the speed and the cost of response.

For the pandemic mitigation testbed, the baseline scenario proved that a no-intervention approach has significant economic impacts on the system by allowing a rapid uprising in the peak of infected individuals and increment of the medical treatment and healthcare services costs. However, more aggressive approaches to containing virus spread also proved

to involve considerable economic effects on the population's individuals since they suggest extended periods of isolation and school and workplace closures. Longer periods imply losses in the community's productivity. So, chasing resilience improvement without regard to costs is meaningless. In that sense, the optimal policy recommends a moderate intervention to reduce the infected number and minimize the costs.

7.3 Contributions

This research's first contribution aims to present a broader framework for resilience enhancement by considering standard parameters in the resilience literature and focusing on disruption mitigation and a system's recovery response. The framework enables a comprehensive approach to understanding the dynamics of a system's resilience by modeling the post-disruption response as a Markov process. Moreover, thanks to the multiple waves' dynamic in our pandemic outbreak testbed, we also proved that the framework provides the basics for incorporating multiple disruptions scenarios in decision-making.

Secondly, we offer a suitable function to quantify resilience costs by considering the costs of intervention and the costs of having a disrupted system with partial performance. We incorporated this function into our CTMDP model to balance the costs of resilience and derived the optimal policy for both testbeds that ensures acceptable resilience levels with minimal cost.

Finally, we also remark that a dynamic stochastic approach enables proactive decision support to allocate system resources for the post-disruption mitigation process. Stochastic dynamic modeling is better than static deterministic models because it fits the random behavior of a resilience dimension, such as the recovery time. Furthermore, it allows a decision-maker to select the best possible action for different scenarios.

7.4 Future Research and Model Limitations

The proposed stochastic optimization model aims to enhance the overall resilience assessment of a system by improving either the disruption mitigation or the recovery process. Nonetheless, a broader approach should integrate both resilience dimensions (absorptive and recovery) in the system's response.

The most straightforward path to address this problem seems to incorporate mitigation actions to reduce the performance losses and allow backward transitions into the model. This approach implies the necessity of a transition rate function that helps the model decide those states where it is better to allocate resources for mitigation rather than recovery. Furthermore, we may need to consider the disruption intensity to build this transition rate function. This function may work as a sort of balance equation such that depending on the difference between the intensity and resources to allocate for a particular state, the probability of a forward (recovery) or a backward (mitigation) transition may change. However, the disruption intensity will add new challenges to this problem since it is time-dependent and transforms the model into a non-homogeneous Markov process. To the best of our knowledge, there is no exact solution method for those kinds of models. We could consider disruption intensity constant for long-lasting disruption scenarios, but there is no guarantee to derive an optimal policy.

References

[1] D. Romero-Rodriguez, A. Savachkin, W. Ardila-Rueda, A. Sierra-Altamiranda, and J.-M. Daza-Escorcia, "Multi-stage recovery resilience: A case study of the dique canal," in *International Conference on Computational Logistics*, pp. 428–442, Springer, 2019.

[2] L. Herrera-Delhas, "El dique: 10 años de la tragedia que inundó el sur del atlántico," 2020.

[3] D. Romero Rodriguez, "Physical and social systems resilience assessment and optimization," 2018.

[4] D. Romero Rodriguez, W. Silva, A. Savachkin, T. Das, and J. Daza, "Resilience as a measure of preparedness for pandemic influenza outbreaks," *Health Systems*, pp. 1–10, 2022.

[5] A. Savachkin and A. Uribe, "Dynamic redistribution of mitigation resources during influenza pandemics," *Socio-Economic Planning Sciences*, vol. 46, no. 1, pp. 33–45, 2012.

[6] C. W. Zobel, "Representing perceived tradeoffs in defining disaster resilience," *Decision Support Systems*, vol. 50, no. 2, pp. 394–403, 2011.

[7] M. Bruneau, S. E. Chang, R. T. Eguchi, G. C. Lee, T. D. O'Rourke, A. M. Reinhorn, M. Shinozuka, K. Tierney, W. A. Wallace, and D. Von Winterfeldt, "A framework to quantitatively assess and enhance the seismic resilience of communities," *Earthquake spectra*, vol. 19, no. 4, pp. 733–752, 2003.

[8] A. Rose, "Covid-19 economic impacts in perspective: A comparison to recent us disasters," *International Journal of Disaster Risk Reduction*, vol. 60, p. 102317, 2021.

[9] M. Xu, X. Wang, and L. Zhao, "Predicted supply chain resilience based on structural evolution against random supply disruptions," *International Journal of Systems Science: Operations & Logistics*, vol. 1, no. 2, pp. 105–117, 2014.

[10] I. Livingston, "What made hurricane ian so intense: By the numbers," 2022.

[11] S. Kermanshachi, K. Bergstrand, and B. Rouhanizadeh, "Identifying, weighting and causality modeling of social and economic barriers to rapid infrastructure recovery from natural disasters: A study of hurricanes harvey, irma and maria," 2019.

[12] J. Winkelmann, E. Webb, G. A. Williams, C. Hernández-Quevedo, C. B. Maier, and D. Panteli, "European countries' responses in ensuring sufficient physical infrastructure and workforce capacity during the first covid-19 wave," *Health Policy*, vol. 126, no. 5, pp. 362–372, 2022.

[13] H. Liu, H. Tatano, G. Pflug, and S. Hochrainer-Stigler, "Post-disaster recovery in industrial sectors: A markov process analysis of multiple lifeline disruptions," *Reliability Engineering & System Safety*, vol. 206, p. 107299, 2021.

[14] R. Guidotti, P. Gardoni, and N. Rosenheim, "Integration of physical infrastructure and social systems in communities' reliability and resilience analysis," *Reliability Engineering & System Safety*, vol. 185, pp. 476–492, 2019.

[15] H. Sun, Y. Wang, and Y. Xue, "A bi-objective robust optimization model for disaster response planning under uncertainties," *Computers & Industrial Engineering*, vol. 155, p. 107213, 2021.

[16] C. A. MacKenzie and C. W. Zobel, "Allocating resources to enhance resilience, with application to superstorm sandy and an electric utility," *Risk Analysis*, vol. 36, no. 4, pp. 847–862, 2016.

[17] T. K. Das, A. A. Savachkin, and Y. Zhu, "A large-scale simulation model of pandemic influenza outbreaks for development of dynamic mitigation strategies," *Iie Transactions*, vol. 40, no. 9, pp. 893–905, 2008.

[18] D. L. Martinez and T. K. Das, "Design of non-pharmaceutical intervention strategies for pandemic influenza outbreaks," *BMC public health*, vol. 14, no. 1, pp. 1–14, 2014.

[19] S. Galaitsi, J. M. Keisler, B. D. Trump, and I. Linkov, "The need to reconcile concepts that characterize systems facing threats," *Risk Analysis*, vol. 41, no. 1, pp. 3–15, 2021.

[20] D. Chua and Y. M. Goh, "Poisson model of construction incident occurrence," *Journal of Construction Engineering and Management*, vol. 131, no. 6, pp. 715–722, 2005.

[21] G. P. Cimellaro, A. M. Reinhorn, and M. Bruneau, "Framework for analytical quantification of disaster resilience," *Engineering structures*, vol. 32, no. 11, pp. 3639–3649, 2010.

[22] C. W. Zobel, "Comparative visualization of predicted disaster resilience," in *Proceedings of the 7th International ISCRAM Conference*, pp. 1–5, ISCRAM, 2010.

[23] C. W. Zobel and L. Khansa, "Characterizing multi-event disaster resilience," *Computers & Operations Research*, vol. 42, pp. 83–94, 2014.

[24] M. Ouyang, L. Dueñas-Osorio, and X. Min, "A three-stage resilience analysis framework for urban infrastructure systems," *Structural safety*, vol. 36, pp. 23–31, 2012.

[25] M. Ouyang and L. Duenas-Osorio, "Multi-dimensional hurricane resilience assessment of electric power systems," *Structural Safety*, vol. 48, pp. 15–24, 2014.

[26] P. Bocchini and D. M. Frangopol, "Optimal resilience-and cost-based postdisaster intervention prioritization for bridges along a highway segment," *Journal of Bridge Engineering*, vol. 17, no. 1, pp. 117–129, 2012.

[27] C. Rougé, J.-D. Mathias, and G. Deffuant, "Extending the viability theory framework of resilience to uncertain dynamics, and application to lake eutrophication," *Ecological indicators*, vol. 29, pp. 420–433, 2013.

[28] R. Pant, K. Barker, J. E. Ramirez-Marquez, and C. M. Rocco, "Stochastic measures of resilience and their application to container terminals," *Computers & Industrial Engineering*, vol. 70, pp. 183–194, 2014.

[29] B. M. Ayyub, "Practical resilience metrics for planning, design, and decision making," *ASCE-ASME Journal of Risk and Uncertainty in Engineering Systems, Part A: Civil Engineering*, vol. 1, no. 3, p. 04015008, 2015.

[30] X. Zhang, E. Miller-Hooks, and K. Denny, "Assessing the role of network topology in transportation network resilience," *Journal of Transport Geography*, vol. 46, pp. 35–45, 2015.

[31] D. L. Alderson, G. G. Brown, and W. M. Carlyle, "Operational models of infrastructure resilience," *Risk Analysis*, vol. 35, no. 4, pp. 562–586, 2015.

[32] L. L. Njilla, C. A. Kamhoua, K. A. Kwiat, P. Hurley, and N. Pissinou, "Cyber security resource allocation: A markov decision process approach," in *2017 IEEE 18th International Symposium on High Assurance Systems Engineering (HASE)*, pp. 49–52, IEEE, 2017.

[33] A. Clark and S. Zonouz, "Cyber-physical resilience: Definition and assessment metric," *IEEE Transactions on Smart Grid*, 2017.

[34] D. Hulse, C. Hoyle, K. Goebel, and I. Y. Tumer, "Optimizing function-based fault propagation model resilience using expected cost scoring," in *ASME 2018 International Design Engineering Technical Conferences and Computers and Information in Engineering Conference*, American Society of Mechanical Engineers Digital Collection, 2018.

[35] O. Kammouh, P. Gardoni, and G. P. Cimellaro, "Probabilistic framework to evaluate the resilience of engineering systems using bayesian and dynamic bayesian networks," *Reliability Engineering & System Safety*, vol. 198, p. 106813, 2020.

[36] H. Liu, H. Tatano, Y. Kajitani, and Y. Yang, "Modelling post-disaster recovery process of industrial sectors: A case study of 2016 kumamoto earthquakes," *International Journal of Disaster Risk Reduction*, p. 102385, 2021.

[37] S. Geng, S. Liu, and Z. Fang, "A demand-based framework for resilience assessment of multistate networks under disruptions," *Reliability Engineering & System Safety*, vol. 222, p. 108423, 2022.

[38] L. Iannacone, N. Sharma, A. Tabandeh, and P. Gardoni, "Modeling time-varying reliability and resilience of deteriorating infrastructure," *Reliability Engineering & System Safety*, vol. 217, p. 108074, 2022.

[39] S. Hosseini, K. Barker, and J. E. Ramirez-Marquez, "A review of definitions and measures of system resilience," *Reliability Engineering & System Safety*, vol. 145, pp. 47–61, 2016.

[40] C. W. Zobel and L. Khansa, "Quantifying cyberinfrastructure resilience against multi-event attacks," *Decision Sciences*, vol. 43, no. 4, pp. 687–710, 2012.

[41] C. A. MacKenzie, H. Baroud, and K. Barker, "Static and dynamic resource allocation models for recovery of interdependent systems: application to the deepwater horizon oil spill," *Annals of Operations Research*, vol. 236, no. 1, pp. 103–129, 2016.

[42] N. U. I. Hossain, F. Nur, S. Hosseini, R. Jaradat, M. Marufuzzaman, and S. M. Puryear, "A bayesian network based approach for modeling and assessing resilience: A case study of a full service deep water port," *Reliability Engineering & System Safety*, vol. 189, pp. 378–396, 2019.

[43] Y. Sarkale, S. Nozhati, E. K. Chong, B. R. Ellingwood, and H. Mahmoud, "Solving markov decision processes for network-level post-hazard recovery via simulation optimization and rollout," in *2018 IEEE 14th International Conference on Automation Science and Engineering (CASE)*, pp. 906–912, IEEE, 2018.

[44] G. Vachtsevanos, B. Lee, S. Oh, and M. Balchanos, "Resilient design and operation of cyber physical systems with emphasis on unmanned autonomous systems," *Journal of Intelligent & Robotic Systems*, vol. 91, no. 1, pp. 59–83, 2018.

[45] E. Serfilippi and G. Ramnath, "Resilience measurement and conceptual frameworks: a review of the literature," *Annals of Public and Cooperative Economics*, vol. 89, no. 4, pp. 645–664, 2018.

[46] X. Guo and O. Hernández-Lerma, *Continuous-time markov decision processes: theory and applications*. Springer-Verlag.

[47] M. L. Puterman, *Markov decision processes: discrete stochastic dynamic programming*. John Wiley & Sons, 2014.

[48] F. Qin, A. Auerbach, and F. Sachs, "Maximum likelihood estimation of aggregated markov processes," *Proceedings of the Royal Society of London. Series B: Biological Sciences*, vol. 264, no. 1380, pp. 375–383, 1997.

[49] A. M. Sánchez-Jabba, "Después de la inundación," *Documentos de Trabajo Sobre Economía Regional y Urbana; No. 150*, 2011.

[50] L. Zulaica and F. Oriolani, "Quality of life and habitability conditions in peri-urban areas of southern mar del plata, argentina: a multimethod study," *Applied Research in Quality of Life*, vol. 14, no. 3, pp. 659–683, 2019.

[51] S. Salem, A. Siam, W. El-Dakhakhni, and M. Tait, "Probabilistic resilience-guided infrastructure risk management," *Journal of Management in Engineering*, vol. 36, no. 6, p. 04020073, 2020.

[52] A. U. Abdelhady, S. M. Spence, and J. McCormick, "A framework for the probabilistic quantification of the resilience of communities to hurricane winds," *Journal of Wind Engineering and Industrial Aerodynamics*, vol. 206, p. 104376, 2020.

[53] T. P. Minka, "Estimating a gamma distribution," *Microsoft Research, Cambridge, UK, Tech. Rep*, 2002.

[54] N. Qualls, A. Levitt, N. Kanade, N. Wright-Jegede, S. Dopson, M. Biggerstaff, C. Reed, A. Uzicanin, C. C. M. G. W. Group, C. C. M. G. W. Group, *et al.*, "Community mitigation guidelines to prevent pandemic influenza—united states, 2017," *MMWR Recommendations and Reports*, vol. 66, no. 1, p. 1, 2017.

[55] N. Shrestha, M. Y. Shad, O. Ulvi, M. H. Khan, A. Karamehic-Muratovic, U.-S. D. Nguyen, M. Baghbanzadeh, R. Wardrup, N. Aghamohammadi, D. Cervantes, *et al.*, "The impact of covid-19 on globalization," *One Health*, vol. 11, p. 100180, 2020.

[56] J. Bonet-Morón, D. Ricciulli-Marín, G. J. Pérez-Valbuena, L. A. Galvis-Aponte, E. A. Haddad, I. F. Araújo, and F. S. Perobelli, "Regional economic impact of covid-19 in colombia: An input–output approach," *Regional Science Policy & Practice*, vol. 12, no. 6, pp. 1123–1150, 2020.

[57] J. Cuesta and J. Pico, "The gendered poverty effects of the covid-19 pandemic in colombia," *The European journal of development research*, vol. 32, no. 5, pp. 1558–1591, 2020.

[58] F. Ball, C. Larédo, D. Sirl, and V. C. Tran, *Stochastic Epidemic Models with Inference*, vol. 2255. Springer Nature, 2019.

[59] G. Cacciapaglia, C. Cot, and F. Sannino, "Multiwave pandemic dynamics explained: How to tame the next wave of infectious diseases," *Scientific reports*, vol. 11, no. 1, pp. 1–8, 2021.

About the Author

Weimar A. Ardila-Rueda was born in Barranquilla, Colombia, in July 1991. He got both his bachelors' degree in industrial engineering and master's degree in management systems from the Universidad Autónoma del Caribe in Colombia in 2013 and 2015, respectively. Currently, he is pursuing his Ph.D. degree in industrial engineering from the University of South Florida in the United States.

He has publications related to risk management and resilience assessment, and decision support models applications. His research interests are focused on Applied statistics and stochastic modeling, predictive analytics and machine learning applications, and resilience improvement for emergency planning and pre- and post-disaster intervention.

Mr. Ardila-Rueda is a member of the Institute for Operations Research and Management Sciences (INFORMS). In addition, he held the president position of the INFORMS student chapter of the University of South Florida during the academic year 2020-21.